ALTERNATIVE CLOSURE OF THE YVON-BORN-GREEN HIERARCHY

by

Sina Zare Pakzad

B.S., Mechanical Engineering, University of Tabriz, 2014

Submitted to the Institute for Graduate Studies in
Science and Engineering in partial fulfillment of
the requirements for the degree of
Master of Science

Graduate Program in Mechanical Engineering

Boğaziçi University

2017

ACKNOWLEDGEMENTS

Working under supervision of Prof. Jeremy Mason and Prof. Hakan Ertürk was a valuable experience for me. Prof. Mason was not only a patient and incredible mentor but also a teacher with such a friendly approach toward students. This research would not have been possible without his guidance and encouragement. I find myself more that lucky to find the chance to work with my advisors for more that two years.

I would like to acknowledge my thesis committee, Prof. Nazlı Dönmezer and Prof. Güney Güven Yapıcı for devoting their valuable time to read and comment on my thesis.

I have a long list of friends who made my stay at the beautiful Istanbul unforgettable. To name a few, I would mention Sina Mousazadeh, Siamak Vajdi, Pouya Yousefi, Sina Ahmadvash, Amin Delparish, Seyed Mehdi Emadian, Aydin Sheikhi, Mehdi Madani, Çağlar Şahin, Gökhan Kıyak, Erdem Eren and Tolga Akiner.

Last but not least my special love and gratitude to my family who borne a lot so I can achieve what I've gained so far, to my lovely mom Mahnaz to my kind dad Ali and to my sisters Ferinaz and Faranak, who are also my good friends.

ABSTRACT

ALTERNATIVE CLOSURE OF THE YVON-BORN-GREEN HIERARCHY

Lacking an efficient operation on the correct time scales has caused atomistic level simulation methods to encounter some limitations as they can not study phenomenas like phase transition. One of the obstacles in achieving convincing results is unsound theory, which is the fundamental in atomistic level simulations. Another issue is restriction to specific types of interaction which limits the overall simulation length. In order to study the phase change, we have developed a novel model which provides an accurate evolution equation for atomic systems with arbitrary interatomic potentials on diffusive time scales. This method can be alternative to available simulation methods in this branch of study which are molecular dynamics, dynamical density functional theory and phase field crystal model. The method provides the one-body distribution function in a closed form with explicit interatomic potential and is able to model the behavior of crystals on atomic length scales and leads to simulations that are many orders of magnitude times faster than other approaches. By using this approach, the crystal structure and properties could be specified directly without deriving a free-energy functional as for DDFT, or fitting the coefficients in the gradient-expansion of the direct correlation function as for the PFCM. Method could be extended to construct a phase diagram for the given interatomic potential and applied to longer times to follow the nucleation and growth of a crystal from the initially disordered solid. This method can have the ability to model other crystal structures with more diverse kinetic phenomena like diffusion. The result of this thesis is intended to more accurately reproduce the atomic behavior of solids and liquids as observed by molecular dynamics simulations.

ÖZET

YVON-BRON-GREEN HİYERARŞİSİNİN ALTERNATİF KAPALILIĞI

Doğru zaman ölçeğinde verimli bir işlem eksikliği, atom düzeyindeki simülasyon yöntemlerinin bazı kısıtlarla karşılaşmasına neden olmakta ve faz dönüşümü gibi olaylar çalışılamamaktadır. Tatmin edici sonuçların elde edilmesindeki engellerden biri, atom düzyindeki simülasyonlarda temel olan teorinin güçsüz olmasıdır. Bir diğer mesele ise tüm simülasyon uzunluğunu daraltan belirli bir türdeki etkileşimin sınırlanmasıdır. Faz dönüşümünün çalışılması için yaygın zaman ölçeğinde, isteğe bağlı atomlar arası potansiyelli atomsal sistemler için kesin bir dönüşüm denklemi sağlayan yeni bir model geliştirdik. Bu model, moleküler dinamik, dinamik yoğunluk fonksiyon teorisi ve faz alanı kristal model alanlarıda mevcut simülasyon yöntemlerine bir alternatif olabilir. Bu model kapalı yapıda açık atomlar-arası potansiyelli bir-hacim dağılım fonksiyonu sağlamaktadır ve atomik boyutsal ölçekte kristal davranışlarını modelleyebilmekte ve diğer yaklaşımlardan çok daha hızlı simülasyonları sağlayabilmektedir. Bu yaklaşımı kullanarak kristal yapısı ve özellikleri, DDFT yöntemindeki gibi serbest-enerji fonksiyonu türetmeden veya PFCM yöntemindeki gibi direkt korelasyon fonksiyonunun gradyan genişlemesi katsayıları arasında eğri uydurmadan, direkt olarak belirlenebilmektedir. Bu yöntem, verilen atomlar-arası potansiyel için bir faz diyagramı oluşturmak için genişletilebilmekte, bir kristalin düzensiz katı halden itibaren çekirdeklenmesini ve büyümesini takip etmek için uygulanabilmektedir. Ayrıca bu yöntem başka kristal yapıların difüzyon gibi daha değişik kinetik özelliklerini modelleme yeteneğine de sahip olabilmektedir. Bu tezin sonuçları ile, moleküler dinamik simülasyonları ile incelenen katı ve sıvıların atomik davranışlarının daha hassas bir biçimde yeniden incelenmesi tasarlanmıştır.

TABLE OF CONTENTS

LIST OF FIGURES

LIST OF TABLES

LIST OF ACRONYMS/ABBREVIATIONS

PFCM	Phase Field Crystal Model
PFC	Phase Field Crystal
DFT	Density Functional Theory
DDFT	Dynamical Density Functional Theory
MT	Marconi and Tarazona
MD	Molecular Dynamics
YBG	Yvon-Born-Green
LAMMPS	Large-scale Atomic/Molecular Massively Parallel Simulator
VMD	Visual Molecular Dynamics
PT	Pressure - Temperature

LIST OF SYMBOLS

c	Direct correlation function
g	Radial distribution function
g^n	Correlation function
h	Total correlation function
k	Boltzmann constant
z	Activity
A	Area
E	Energy
F	Force
N	Molecules of a single component
P	Distribution function
T	Temperature
U	Internal energy
V	Volume
Z	Configuration integral
β	1/KT
ξ	Coupling Parameter
$\rho(\mathrm{r})$	Ensemble averaged density
$\bar{\rho}(\mathrm{r})$	One body density
ψ	External potential
Λ	Chemical activity
Ξ	Grand canonical partition function

1. INTRODUCTION

This thesis is concerned with the simulation of atomic motion. The standard approach is molecular dynamics (MD), but this requires short time steps on the scale of the atomic vibration period and limits the overall simulation length. One approach to overcome this is to use statistical mechanics to follow only the average particle motion. However, the resulting equations are either restricted to very specific particle systems, as for dynamic density functional theory (DDFT), or are theoretically unsound, as for the phase field crystal model (PFCM).

In statistical mechanics, the YBG (Yvon-Born-Green hierarchy) is a set of equations describing the dynamics of a system of a large number of interacting particles. The equation which describes the probability density function for the positions of a specific number of particles depends on the equations for higher numbers of particles, resulting in a hierarchy. This thesis proposes an alternative closure of the hierarchy to simulate the evolution of the one-body distribution function as a function of time. This is envisioned as an alternative to DDFT applied to colloidal liquids, and to PFCM for crystalline solids.

The advantage of the present formulation is that the terms of the interatomic potential appear explicitly in the evolution equation for the one-body distribution function. This allows the crystal structure and properties to be specified directly without deriving a free-energy functional as for DDFT, or fitting the coefficients in the gradient-expansion of the direct correlation function as for the PFCM. The result is intended to more accurately reproduce the atomic behavior of solids and liquids as observed by molecular dynamics simulations.

Section 2.1 briefly reviews the derivation and applications of DDFT and PFCM. The limitations and applicability of these methods for the simulation of realistic systems is also discussed. Section 2.2 provides the theoretical background necessary to discern the similarities and differences with existing approaches. Section 3 performs molecular

dynamics (MD) simulations to predict the temperature range of the melting point of copper with the selected interatomic potential. Section 4 introduces the alternative closure that is central to this thesis, and which is expected to give a more theoretically sound evolution equation for the one-body distribution function. Section 5 shows that phase transition and solidification phenomena can be visualized using the method introduced in Section 4. The appendices include specific equations for three-body potentials, various mathematical relations necessary to simplify and derive the final equations, and MATLAB codes for the calculation of the various distribution functions.

2. LITERATURE SURVEY

2.1. Literature Review

There are three major existing approaches to studying the motion of many-particle systems. These are dynamic density functional theory, the phase field crystal model, and molecular dynamics. The capabilities and limitations of these three methods are reviewed below.

2.1.1. Dynamical Density Functional Theory

Density functional theory (DFT) is extensively used to study the static properties of particulate systems [1, 2]. This formalism considers the particle density to be the fundamental variable [3] and defines the state of the system in terms of the particle density. In the context of equilibrium statistical mechanics, this allows one to replace the complicated grand canonical free energy of a system by a much simpler functional of the one-body particle density $\rho(r)$. The one-body density is estimated by minimizing the energy functional with respect to functional variations. The many variations of this basic computational scheme are collectively called DFT [4–7]. Usually DFT is not exact because the actual free energy functional is unknown [8–10], but it is still the most accurate method available in many situations.

Historically, research investigating dynamic DFT has focused on microscopic equations of motion that allow deeper insight into off-equilibrium situations [11–13]. Two new and important studies by Tarazona et al. and Archer et al. develop the DDFT by evaluating the particle density $\rho(r, t)$ as a function of time, but differ in how the authors define $\rho(r, t)$ [2, 4, 5, 14].

The first procedure of Marconi and Tarazona (MT) [2,14] is based on some earlier results of Evans and Dieterich [4,5,15,16]. By means of an approximate closure the au-

thors derive a deterministic equation for the average particle theory from the Langevin stochastic equations. The approximate closure assumes that the equal-time two point correlation function has the same properties in equilibrium and out of equilibrium. This allows the derivation of a DDFT starting from the stochastic equations of particle motion, and has been validated by comparing the DDFT and averages over Langevin simulations. Moreover, Tarazona's continuity equation agrees with a Fokker-Planck equation for the probability distribution of the density published in a separate sets of papers by Kawasaki [12, 13]

The above derivation assumes that the system obeys relaxational dynamics where the velocity distribution is negligible [2, 14]. More specifically, this approach is based on the stochastic Brownian equations of motion for a system of particles with two-body interactions. However, the equilibrium statistical ensemble for the Brownian and Newtonian equations can be very different in some cases, particularly for systems where the microscopic dynamics is Newtonian. Systems that obey the Brownian equation of motion necessarily involve particles significantly larger than individual atoms, e.g., colloidal particles in a bath [2, 14].

The second procedure to obtain a DDFT begins from the one-body density profile of the fluid $\bar{\rho}(r,t)$, as distinguished from the ensemble averaged density $\rho(r,t)$. The starting point of this derivation is the Smoluchaowski equation where the particles interact by Brownian dynamics. The main approximation is that the equilibration between momentum degrees of freedom is faster than that between the positional degrees of freedom. This makes the theory much more relevant to colloidal fluids than to molecular fluids. This assumption is more reasonable particularly for high density fluids where each of particle has many neighbors and the momentum degrees of freedom can equilibrate more quickly [4, 5].

Most recent DDFT studies are related to colloidal fluids. These include dense suspensions of colloidal hard spheres [17], modeling diffusion in colloidal suspensions [18], sedimentation of a two-dimensional colloidal mixture [19], and vacancy diffusion in colloidal crystals [20]. Note that while the DDFT is highly accurate, it is limited to

specific types of interactions and is mainly used for hard spheres and hard rods.

2.1.2. Phase Field Crystal Model

The phase field crystal method (PFCM) is a recent continuum modeling approach that is used to model crystalline phenomena at the atomistic length scales and diffusive time scales [21]. That is, the PFCM has the same spatial resolution as molecular dynamics but is able to study longer time scales [21, 22]. This method was introduced by Elder et al. [22–24] and adapts the mathematical machinery of the phase field model to the atomic scale [23, 25]. Phase field crystal simulations use a single conserved order parameter (density field) to represent the time averaged atomic density, and postulates a free energy functional which is minimized by periodic density fields to define the dynamics. The basic concepts of the PFCM and some main applications have been reviewed in Ref [26].

Phenomena studied include, e.g. solidification [27], elastic deformation [28], behavior of grain boundaries [29], structural phase transformation [30, 31], and spinodal decomposition [32]. A thorough study by Emmerich et al. reviewed about 200 publications on PFCM, the derivation of the model and various applications [33]. The PFCM is based on the Swift-Hohenberg equation [34] and was originally used to model phase transformations in periodic systems, including crystalline solids [24]. Elder et al. [24] reports the similarity of PFCM and the atomic density function theory of Jon and Khachaturyan [35], and emphasizes that the ability to work on diffusive time scales instead of the small time scales associated with lattice vibrations is the main advantage of this approach. One of the main applications of PFCM is the coexistence of solid-liquid phases and solidification phenomena, as reviewed in separate articles by Humadi et al. and Asadi et al. [36, 37]. These also include the classification of phase diagrams of different phase field crystal models such as One-Mode PFCM, Two-Mode PFCM and other PFC Models [37, 38].

Frequent themes of structural phase transitions, solidification [22], and stable dislocations [39] in PFCM articles suggest that the configuration of nearest neighbors

and the evolution of this configuration is important to their conclusions. To compare the relative merits of DDFT and PFCM, a derivation of the PFCM for colloidal solidification is provided by Sven van Teeffelen and Rainer Backofen [27].They show that the PFCM describes the qualitative aspects of crystal growth reliably but lacks precision. Another comparison of the DDFT and PFCM showed that the descriptions of crystal-fluid interfaces and hard-sphere crystals in the PFCM predicted several quantities incorrectly and identified other issues relating to the order parameter [40]. They suggest a procedure to find the PFC parameters, but unless the structure factor and coexistence free energies can be fitted well the issue with the order parameter remains.

Briefly, the literature suggests that the PFCM can be used to model many different phenomena, but is often inaccurate. Furthermore, the PFCM only allows limited atomic interactions via the adjustable parameters, restricting crystal structures to those enumerated in Ref [41].

2.1.3. Molecular Dynamics

Molecular dynamics (MD) is a simulation tool to study a variety of phenomenas on the atomic scale using Newton's laws of motion. They are often be used to enhance our understanding of atomic phenomena that are difficult to observe experimentally. The positions and momenta of the constituent atoms can be found by various algorithms including, e.g. the velocity Verlet, Verlet leapfrog, and Gear predictor-corrector algorithms [42, 43]. The MD method was first used in the statistical mechanics simulations of Alder and Wainwright [44], and since then has found broad application in different branches of science (including mechanical engineering, material sciences, chemistry and other disciplines) [45–48].

Molecular dynamics models the atomic trajectories as evolving from an initial configuration by means of specified atomic interactions [42, 49, 50]. The selection of an appropriate interatomic potential is crucial to the results of MD simulations, but can be constrained by computational expense or other systematic limitations. The essen-

tial ingredients of a molecular dynamics simulation and the available intermolecular potentials have been reviewed by Allen et al. (2004) [51]. A serious weakness of this method is the limitation to material phenomena where the effect of electron transport is negligible because this model does not include the details of electron positions and momenta [42]. Another limitation reported in the literature is the restriction to classical equations of motion, and a considerable literature has investigated various quantum corrections [42, 52].

2.2. Theoretical Background

This section summarizes the basic definitions and equations required to derive our main results in Section 4.

2.2.1. Statistical Mechanics

Statistical mechanics is a branch of theoretical physics dealing with the application of statistical principles to the mechanics of a microscopic system. Statistical mechanics traditionally describes systems in equilibrium, and is otherwise called statistical thermodynamics. Some progress has been made for non-equilibrium systems, though this is one of the most difficult parts of the field both theoretically and mathematically. The definition of the system plays a significant role in the theory, and requires the concept of an ensemble as introduced by J. Willard Gibbs [6, 53, 54].

2.2.2. Ensemble of the System

An ensemble is a collection of a large number of nominally identical systems. The systems in the ensemble are all characterized by some number of compatible thermodynamic quantities, like the number of molecules of a single component N, the volume V, and the temperature T. The ensemble has a total volume and number of atoms equal to the values of a single system multiplied by the number of systems.

Different types of ensembles are useful depending on the application. Whether the ensemble is a microcanonical ensemble, canonical ensemble, grand canonical ensemble, etc., depends on the fixed quantities of the system [54]. An ensemble with fixed N, V, and E is called the micro canonical ensemble, and is commonly used in theoretical discussions and molecular dynamics simulations. An ensemble with N, V, and T fixed is called the canonical ensemble and is commonly used in statistical mechanics. If each system in the canonical ensemble is open with respect to the transport of matter, the result is called the grand canonical ensemble.

2.2.3. Distribution Functions

In the study of liquids, distribution functions are a concept of central importance. According to the definition of a distribution function in a system with N particles, volume V, and temperature T, the joint probability that molecule 1 is in dr_1 (an infinitesimal volume element) around r_1, that molecule 2 is in dr_2 around r_2, ..., and that molecule n is in dr_n around r_n, irrespective of the configuration of the remaining $N - n$ molecules, is the n-particle probability

$$P^{(n)}(r_1, ..., r_n) = \frac{\int \cdots \int e^{-\beta U_N} dr_{n+1} \ldots dr_N}{Z_N} \tag{2.1}$$

where Z_N is the configuration integral, U_N is the potential energy due to particle interactions, and $\beta = \frac{1}{kT}$. The probability that *any* molecule is in dr_1 (an infinitesimal volume element) at r_1, that *any* molecule is in dr_2 at r_2, ..., and that *any* molecule is in dr_n at r_n, irrespective of the configuration of the remaining $N - n$ molecules, is

$$\rho^{(n)}(r_1, ..., r_n) = \frac{N!}{(N-n)!} P^{(n)}(r_1, ..., r_n). \tag{2.2}$$

The integral of the one-particle density for an equilibrium fluid is equal to the overall density ρ of the system since

$$\frac{1}{V}\int \rho^{(1)}(r_1)\ dr_1\ = \frac{N}{V} = \rho. \tag{2.3}$$

A correlation function $g^{(n)}$, which describes the variation of the density as a function of distance from a reference particle is defined as [54]

$$\rho^{(n)}(r_1, ..., r_n) = \rho^n g^{(n)}(r_1, ..., r_n). \tag{2.4}$$

Using the above equations, $g^{(n)}$ can be written as

$$g^{(n)}(r_1, ..., r_n) = \frac{V^n N!}{N^n (N-n)!} \cdot \frac{\int \cdots \int e^{-\beta U_N} dr_{n+1} \dots dr_N}{Z_N} \tag{2.5}$$

In a spherically symmetric liquid $g^{(2)}(r_1, r_2)$ only depends on the relative distance of molecules 1 and 2, e.g. r_{12}. Distribution function $g(r)$, which describes how density varies as a function of distance from a reference particle, can be defined using the above mentioned correlation function. We denote r_{12} simply by r and drop the superscript 2 to write $g^{(2)}(r_1, r_2) = g(r)$. There are several approaches to explicitly calculate approximate radial distribution functions, for instance, the Yvon-Born-Green equation and the Kirkwood integral equation [6, 53–55].

2.2.4. Kirkwood Integral Equation

One of the first and main approximations for $g(r)$ was introduced in the 1930s by John G. Kirkwood [6,53,54]. To derive the Kirkwood equation, begin by modifying Equation 2.2 to introduce a coupling parameter ξ that governs the interaction of particle 1 and every other particle in the system, and the dependence of $\rho^{(n)}$ on particle position

is indicated by 1, 2, ..., n instead of r_1, r_2, ..., r_n.

$$\rho^{(n)}(1,2,...,n;\xi) = \frac{N!}{(N-n)!}.\frac{\int\cdots\int e^{-\beta U(\xi)}dr_{n+1}\dots dr_N}{Z_N(\xi)}. \tag{2.6}$$

Differentiating this equation with respect to ξ according to Ref. [54] gives

$$\begin{aligned} kT\frac{\partial\rho^{(n)}}{\partial\xi} =& \frac{\rho^{(n)}}{Z_N(\xi)}\sum_{j=2}^{N}\int\cdots\int e^{-\beta U(\xi)}u(r_{1j})dr_1\dots dr_N \\ &- \frac{N!}{(N-n)!}\frac{1}{Z_N(\xi)}\sum_{j=2}^{N}\int\cdots\int e^{-\beta U(\xi)}u(r_{1j})dr_{n+1}\dots dr_N \end{aligned} \tag{2.7}$$

where the first term comes from differentiating the denominator of Equation 2.6, and the second term comes from differentiating the numerator. $u(r_{1j})$ is the pairwise interaction of particle 1 with the jth particle of the system.

For the case of a fluid and for n = 2, Equation 2.7 can be written as mentioned in Ref. [54] :

$$\begin{aligned} -kT\ln g^{(2)}(1,2,\xi) = \xi u(r_{12}) + \rho\int_0^{\xi}\int_V u(r_{13})\Bigg[\frac{g^{(3)}(1,2,3,\xi)}{g^{(2)}(1,2,\xi)} \\ - g^{(2)}(1,3,\xi)\Bigg]\,dr_3\,d\xi. \end{aligned} \tag{2.8}$$

The main assumption in the Kirkwood equation is that the triplet correlation can be written as a product of pair-wise independent probabilities, which is called the superposition approximation

$$g^{(3)}(1,2,3) \approx g^{(2)}(1,2)g^{(2)}(1,3)g^{(2)}(2,3). \tag{2.9}$$

Inserting Equation 2.9 into Equation 2.8 gives the final Kirkwood equation for $g(r)$ [54]:

$$-kT\ln g(r_{12},\xi) = \xi u(r_{12}) + \rho\int_0^{\xi}\int_V u(r_{13})g(r_{13};\xi')[g(r_{23})-1]\,dr_3\,d\xi'. \tag{2.10}$$

2.2.5. Yvon-Born-Green Integral Equation

As mentioned in Sections 3.3 and 3.4, the YBG hierarchy is similar to the Kirkwood equation. The main difference is that the gradient of $\rho^{(n)}$ is taken with respect to one of the r_1, ... , r_n rather than with respect to one of the ξ_i [6, 53, 54].

The derivation of the Yvon-Born-Green equation starts by considering any given configuration r_1, ...,r_N of the N molecules of the system. By using Equation 2.1 and Equation 2.2 and the superposition approximations for an open system, $\rho^{(n)}(r_1, ..., r_n)$ is defined as [53]

$$\rho^{(n)}(r_1, ..., r_n) = \frac{1}{\Xi} \sum_{N \geq n} \frac{z^N}{(N-n)!} \int \cdots \int_V e^{-U_N/kT} dr_{n+1} ... dr_N \tag{2.11}$$

where z is the activity and Ξ is the grand canonical partition function.

The Yvon-Born-Green integral equation is found by assuming that particle 1 interacts with the rest of the system only by a pair potential, as in Ref. [53]:

$$\boldsymbol{\nabla}_1 U_N = \sum_{i=2}^{N} \boldsymbol{\nabla}_1 u(r_{1i}). \tag{2.12}$$

Breaking up the sum gives the result

$$-kT \boldsymbol{\nabla}_1 \rho^{(n)} = \frac{1}{\Xi} \sum_{N \geq n} \frac{z^N}{(N-n)!} \int \cdots \int_V e^{-U_N/kT} \boldsymbol{\nabla}_1 U_N dr_{n+1} ... dr_N. \tag{2.13}$$

Equation 2.13 is the YBG intergral equation which relates the pair potential of a simple fluid to the resulting equilibrium two-body correlation functions [56].

2.2.6. Percus-Yevck Equation

The free-energy functional is the total energy of a specific system as a functional of the density of some particle species. The free-energy functional has contributions

from two different parts, one from the ideal-gas part for a noninteracting system of particles and the other (the excess part) from the interaction between the particles. The excess part of the free-energy-functional acts as a generating functional for the direct correlation functions, though this requires functional techniques [54, 57]. An alternative is to define the direct correlation function from an integral equation called the Ornstein-Zernike equation, named after Leonard Ornstein and Frits Zernike. This is used to calculate the interaction between two molecules [53, 55].

The total correlation function is defined as

$$h(r) = g(r) - 1 \tag{2.14}$$

where $g(r)$ is the radial distribution function and $h(r)$ shows the effect of a molecule on another one at a distance r away. The direct correlation function is defined as

$$c(r) = g(r) - g_{indirect}(r). \tag{2.15}$$

where $g_{indirect}(r)$ is the radial distribution function without the direct interaction (defined below).

For a uniform and isotropic fluid, the Ornstein-Zernike relation for the direct correlation function is

$$h(r) = c(r) + \rho \int c(|r - r'|)h(r')dr'. \tag{2.16}$$

Section 3.5 showed that by using an appropriate relation between the distribution function and $g(r)$, one can derive exact equations such as the YBG (Yvon-Born-Green) equations. An approximation given by Percus and Yevick in 1958 equates $g_{indirect}(r)$ with $y(r) = e^{\beta u(r)}g(r)$ in the equation for $c(r)$, giving

$$c(r) = g(r) - y(r) = e^{-\beta u(r)}y(r) - y(r) = f(r)y(r) \tag{2.17}$$

Inserting this approximation into the Ornstein-Zernike equation, the Percus-Yevick (PY) equation is given by

$$y(r_{12}) = 1 + \rho \int f(r_{13}) y(r_{13}) h(r_{23}) dr_3. \tag{2.18}$$

The integral equations that have been discussed are all nonlinear integral equations. The numerical solution of such equations is quite difficult in general [54].

3. PREDICTION OF THE MELTING POINT BY MOLECULAR DYNAMICS

3.1. Overview

This chapter studies the melting point of copper. We perform molecular dynamics (MD) simulations using LAMMPS [58] to determine the temperature range of this phenomena using volume and mean square displacement results. This temperature range, along with the equilibrium volume at fixed pressure and temperature, are used as inputs for the method developed in Chapter 4.

3.2. Method of Simulation

A set of MD simulations were performed at constant temperature and pressure (NPT ensemble) with periodic boundary conditions in 2D. Each simulation contained 2048 atoms and was maintained at a constant pressure of zero MPa. The atoms interacted by a Morse potential obtained from the literature [59, 60]. The simulations were initialized with atoms on a triangular lattice and uniformly distributed random velocities. The displacement of the atoms over the course of the simulation was computed by LAMMPS, and accounted for the effect of the periodic boundary conditions. These simulations were intended to be used to train and validate the model developed in Chapter 4, and for that reason have the same interatomic potential, density, and temperature as the simulations in Chapter 5.

3.3. Computational Details

The pairwise interactions between copper atoms were modeled with a Morse potential. That is, if r_{ij} is the distance between atoms i and j, the interaction energy

is

$$\phi_{ij}(r_{ij}) = D[e^{-2\alpha(r_{ij}-r_0)} - 2e^{-\alpha(r_{ij}-r_0)}] \tag{3.1}$$

where r_0 is the equilibrium separation. The three constants are set to $\alpha = 1.3588$ Å^{-1}, $D = 0.3429$ eV and $r_0 = 2.866$ Å for copper [59, 60]. We used MD to measure the equilibrium volume of copper at temperatures ranging from 300 K to 2300 K in 50 K increments, and the mean square displacement ranging from 300 K to 1600K in 50 K increments. The pressure was controlled with a Berensen barostat with a damping factor of 2.0 to reduce volume oscillations. The command "fix enforce2d" in the configuration file ensured that the z-components of velocity and force variables are zeroed out every time step, and confined the copper atoms to a two-dimension simulation box.

The temperature, instantaneous volume, potential and total energy of the system were recorded for each time step, and visualization of the MD simulations was done using the VMD (Visual Molecular Dynamics) program. The instantaneous and cumulative averages of the system volume at 1350 K are shown in Figure 3.1, and indicate that the volume is equilibrated over 800,000 steps of 1 fs. The inset reports the value of the density as a function of time for the same simulation. While the volume of a system in the NPT ensemble consistently fluctuates about the mean, the cumulative average does not and is used as the converged value.

The resulting volumes and the ratio of their expansions are plotted for different temperatures from 300 K to 2300 K with an increment of 50 K in Figure 3.2. The obvious jump in the volume between 1350 K and 1450 K suggests that the solid to liquid phase transition occurs in this interval.

A similar result is found in Figure 3.3 where the rate of increase of mean square displacement of copper atoms is shown for different temperatures from 300 K to 1600 K with an increment of 50 K. As can be seen from the highlighted region, there is a clear jump in the random displacements of the atoms above 1350 K, supporting the

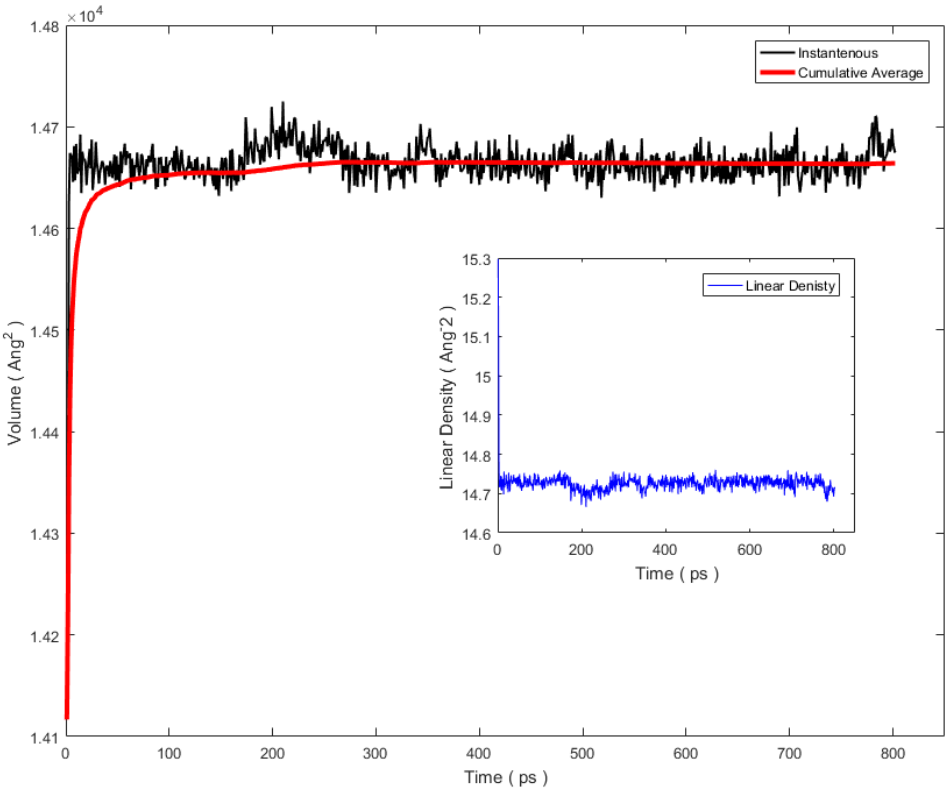

Figure 3.1. Instantaneous and average MD volumes of copper atoms at 1350 K. Inset shows the density vs. simulation time

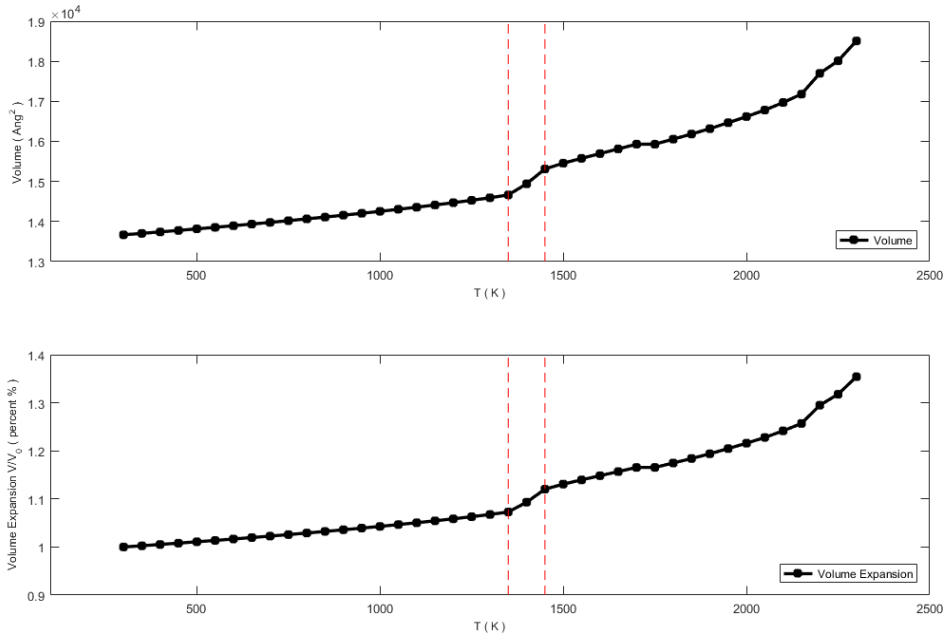

Figure 3.2. Volume and volume expansion plotted vs. temperature. Note the volume increase in temperature range of 1350 K to 1450 K.

existence of a liquid phase with higher atomic mobility around 1400 K.

As a final piece of evidence supporting the existence of a phase transition around 1400 K, Figure 3.4 displays the structures of copper atoms in two dimensions at different temperatures. Observe that the copper atoms adopt a regular close packed (solid) configuration at temperatures below 1400 K, and a much more irregular arrangement with high free volume above 1400 K. Taken with the evidence presented in Figures 3.2 and 3.3, we are confident that our MD simulations have identified a phase transition at 1400 K for pure copper with the specified interatomic potential in two dimensions. The transition temperature and the equilibrium volume at 0 MPa as a function of temperature will be used as inputs for the simulation method presented in the next chapter of this thesis.

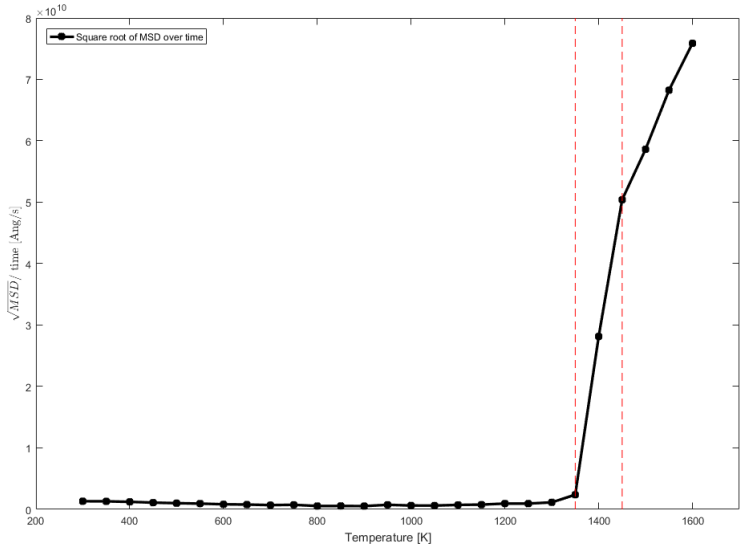

Figure 3.3. Mean square displacement of atoms vs. temperature. Note the highlighted jump in the transition region from 1350 K to 1450 K.

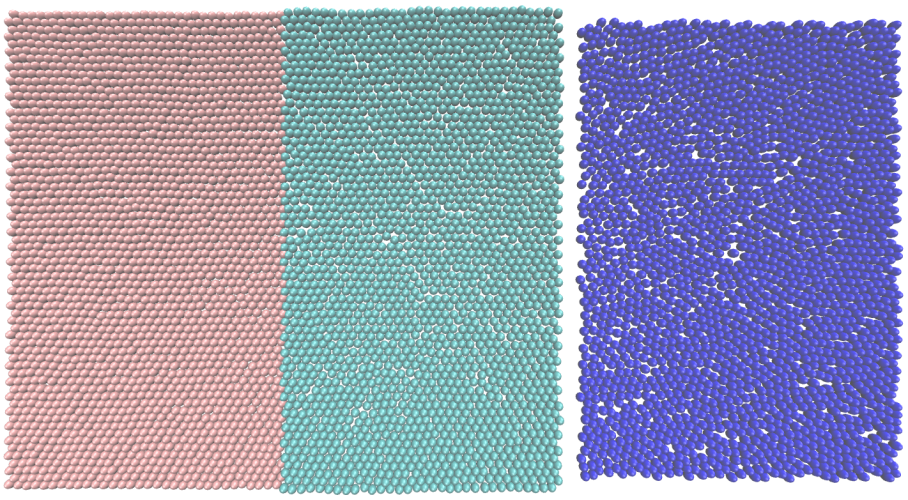

Figure 3.4. Atomic configurations with VMD software at temperatures $T = 700\text{K}, T = 1100\text{K}, T = 1500\text{K}$

4. CURRENT APPROACH

4.1. Introduction

The novel contribution of this thesis is a new closure of the YBG equations which gives a more theoretically-sound one-body distribution function than the existing alternatives.

4.2. Derivation of the Yvon-Born-Green Hierarchy

This section provides a derivation of all the equations in the YBG hierarchy, and uses the grand canonical ensemble for consistency with the derivation of the closure relation in Section 4.3.

The notation merits some discussion. A set of particles is indicated with a bar, and the number of particles in a set is indicated by the same symbol without a bar. Integration variables are defined by a set in parentheses.

The n-body distribution function $p(\bar{n})$ in an equilibrium system in the grand canonical ensemble is

$$p(\bar{n}) = \frac{\sum_{m \geq n} \frac{\Lambda^m}{(m-n)!} \int e^{-\beta[\psi(\bar{m})+U(\bar{m})]} d(\bar{m}-\bar{n})}{\sum_{m \geq 0} \frac{\Lambda^m}{m!} \int e^{-\beta[\psi(\bar{m})+U(\bar{m})]} d(\bar{m})} \tag{4.1}$$

where m is the number of particles in the system, Λ is the chemical activity, $\psi(\bar{m})$ is some external potential, and $U(\bar{m})$ is the internal energy. The external potential $\psi(\bar{m})$ is introduced only to make Equation Equation 4.1 consistent with the currently observed $p(\bar{n})$. While the particles in $\bar{n}$ can be distinguished by location, the indistinguishability of the remaining $m-n$ particles requires the factor of $1/(m-n)!$. The

gradient of the n-body distribution function with respect to the ith particle, where $i \in \bar{n}$, is

$$\boldsymbol{\nabla}_i p(\bar{n}) = -\frac{\beta}{Z} \sum_{m \geq n} \frac{\Lambda^m}{(m-n)!} \int \boldsymbol{\nabla}_i [\psi(\bar{m}) + U(\bar{m})] e^{-\beta[\psi(\bar{m})+U(\bar{m})]} d(\bar{m} - \bar{n}) \tag{4.2}$$

where the normalizing factor in Equation 4.1 is recognized as the partition function Z. Notice that

$$\boldsymbol{\nabla}_i \psi(\bar{m}) = \boldsymbol{\nabla}_i \psi(i) \tag{4.3}$$

since the contribution of the external potential $\psi(\bar{m})$ is the sum of the contributions of individual particles. The gradient of the internal energy is written as

$$\boldsymbol{\nabla}_i U(\bar{m}) = \sum_{\mu \geq 0}^{m-n} \binom{m-n}{\mu} \sum_{\bar{\nu}}^{\bar{n}-i} \frac{1}{\nu!} \boldsymbol{\nabla}_i v(i; \bar{\nu}, \bar{\mu}) \tag{4.4}$$

where $\bar{\mu}$ is the subset of particles in $\bar{m} - \bar{n}$ that interact with the ith atom, $\bar{\nu}$ is the subset of particles in $\bar{n}$ that interact with the ith atom, and $v(i; \bar{\nu}, \bar{\mu})$ is the appropriate interaction potential of the ith atom with $\bar{v}$ and $\bar{u}$. Inserting these in Equation 4.2 and recognizing that $\boldsymbol{\nabla}_i \psi(i)$ is a constant with respect to the integration gives

$$\begin{aligned} \boldsymbol{\nabla}_i p(\bar{n}) = & -\beta p(\bar{n}) \boldsymbol{\nabla}_i \psi(i) \\ & - \frac{\beta}{Z} \sum_{m \geq n} \frac{\Lambda^m}{(m-n)!} \int \sum_{\mu \geq 0}^{m-n} \binom{m-n}{\mu} \sum_{\bar{\nu}}^{\bar{n}-i} \frac{1}{\nu!} \boldsymbol{\nabla}_i v(i; \bar{\nu}, \bar{\mu}) e^{-\beta[\psi(\bar{m})+U(\bar{m})]} d(\bar{m} - \bar{n}). \end{aligned} \tag{4.5}$$

Exchanging the summations over m and μ and expanding the binomial coefficient gives

$$\begin{aligned} \boldsymbol{\nabla}_i p(\bar{n}) = & -\beta p(\bar{n}) \boldsymbol{\nabla}_i \psi(i) \\ & - \frac{\beta}{Z} \sum_{\mu \geq 0} \frac{1}{\mu!} \sum_{m \geq n+\mu} \frac{\Lambda^m}{(m-n-\mu)!} \int \sum_{\bar{\nu}}^{\bar{n}-i} \frac{1}{\nu!} \boldsymbol{\nabla}_i v(i; \bar{\nu}, \bar{\mu}) e^{-\beta[\psi(\bar{m})+U(\bar{m})]} d(\bar{m} - \bar{n}). \end{aligned} \tag{4.6}$$

The quantity $v(i;\bar{\nu},\bar{\mu})$ does not depend on the positions of any of the particles in the set $\bar{m}-\bar{n}-\bar{\mu}$. Performing the integration over the positions of these particles gives

$$\boldsymbol{\nabla}_i p(\bar{n}) = -\beta p(\bar{n})\boldsymbol{\nabla}_i\psi(i) - \beta\sum_{\mu\geq 0}\frac{1}{\mu!}\sum_{\bar{\nu}}^{\bar{n}-i}\frac{1}{\nu!}\int \boldsymbol{\nabla}_i v(i;\bar{\nu},\bar{\mu})p(\bar{n}+\bar{\mu})d(\bar{\mu}). \tag{4.7}$$

This is rearranged to find the force exerted on the ith particle by the external potential $\psi(\bar{m})$ as

$$-\boldsymbol{\nabla}_i\psi(i) = \frac{1}{p(\bar{n})}\left[k_B T\boldsymbol{\nabla}_i p(\bar{n}) + \sum_{\mu\geq 0}\frac{1}{\mu!}\sum_{\bar{\nu}}^{\bar{n}-i}\frac{1}{\nu!}\int \boldsymbol{\nabla}_i v(i;\bar{\nu},\bar{\mu})p(\bar{n}+\bar{\mu})d(\bar{\mu})\right]. \tag{4.8}$$

Since $\psi(\bar{m})$ is defined to make the total force on the particles vanish, the force exerted on the i particle in the absence of the external potential is $\boldsymbol{\nabla}_i\psi(i)$. Assuming a constant mobility Γ, the velocity of the ith particle is

$$\boldsymbol{v}_i = \Gamma\boldsymbol{\nabla}_i\psi(i). \tag{4.9}$$

The requirement that probability density be conserved can be written as

$$\frac{\partial p(\bar{n})}{\partial t} = -\sum_{i}^{\bar{n}}\boldsymbol{\nabla}_i\cdot[p(\bar{n})\boldsymbol{v}_i]. \tag{4.10}$$

Inserting the relevant quantities in the above equation gives

$$\frac{\partial p(\bar{n})}{\partial t} = \Gamma\sum_{i}^{\bar{n}}\boldsymbol{\nabla}_i\cdot\left[k_B T\boldsymbol{\nabla}_i p(\bar{n}) + \sum_{\mu\geq 0}\frac{1}{\mu!}\sum_{\bar{\nu}}^{\bar{n}-i}\frac{1}{\nu!}\int \boldsymbol{\nabla}_i v(i;\bar{\nu},\bar{\mu})p(\bar{n}+\bar{\mu})d(\bar{\mu})\right] \tag{4.11}$$

for the derivative of the n-body distribution function with respect to time. The explicit form of Equation 4.11 depends on n and the assumed potential; for reference, the one-, two- and three-body distribution functions for a system with a three-body potential are provided in Appendix A.

4.3. Alternative Closure

As motivation for this derivation, notice that the intention is to use Equation 4.11 to follow the evolution of the one-body distribution function, as with DDFT and the phase-field crystal model. The usual YBG equations assume that the system is a uniform liquid, meaning that the one-body distribution function is a constant. Historically, this means that closure relations assume that the two-body distribution function is the simplest nontrivial quantity (e.g., the Kirkwood supposition approximation in Equation 2.9), and that the two-body distribution function can be expressed as an expansion with respect to the uniform density about the low-density limit [61]. This means that there is no existing closure for the lowest level of the hierarchy, and that some of the existing approaches will not be useful since the density of the system is explicitly not uniform.

Since any closure at the first level of the hierarchy will necessarily be rather coarse, we attempt to reduce the systematic error as much as possible by effectively expanding around the overall system density. The closure relation proposed below can be considered as the first term of this expansion. The derivation begins with Equation 4.11 for the n-body distribution function. Let $U(\bar{m})$ be separated into one contribution $U(\bar{n})$ containing the interactions among the $\bar{n}$ particles, one contribution $U(\bar{m}-\bar{n})$ containing the interactions among the $\bar{m}-\bar{n}$ particles, and one contribution $U(\bar{n};\bar{m}-\bar{n})$ containing all of the remaining interactions. The exponential of the third contribution can be further separated as

$$\begin{aligned}\exp(-\beta U(\bar{n};\bar{m}-\bar{n})) &= \prod_{i}^{\bar{m}-\bar{n}} \exp(-\beta U(\bar{n};i)) \cdot \prod_{j}^{\bar{m}-\bar{n}} \prod_{k}^{\bar{m}-\bar{n}-j} \exp(-\beta U(\bar{n};jk)) \cdot \ldots \\ &= \prod_{i}^{\bar{m}-\bar{n}} (1+f_{\bar{n};i}) \cdot \prod_{j}^{\bar{m}-\bar{n}} \prod_{k}^{\bar{m}-\bar{n}-j} (1+f_{\bar{n};jk}) \cdot \ldots \end{aligned} \tag{4.12}$$

where $U(\bar{n};i)$ contains all interactions involving any subset of the $\bar{n}$ particles and

exactly the particle $i \in \bar{m} - \bar{n}$, $U(\bar{n}; jk)$ contains all interactions involving any subset of the $\bar{n}$ particles and exactly the two particles $\{j, k\} \subset \bar{m} - \bar{n}$, etc. This means that the functions $f_{\bar{n};i}$ resemble Mayer f-functions [54], but include interactions involving an arbitrary number of particles. Expanding the product in Equation Equation 4.12 gives some sum of products of f-functions. Let $Q(\bar{n}; \bar{\mu})$ be the sum of all terms involving exactly the set of particles $\bar{\mu} \subset \bar{m} - \bar{n}$. Since the indistinguishability of the $\bar{m} - \bar{n}$ particles makes every $Q(\bar{n}; \bar{\mu})$ for a given μ equivalent, Equation 4.12 can be written as

$$\exp(-\beta U(\bar{n}; \bar{m} - \bar{n})) = \sum_{\mu \geq 0}^{m-n} \binom{m-n}{\mu} Q(\bar{n}; \bar{\mu}). \tag{4.13}$$

Separating the contributions to the internal energy as described above allows Equation 4.1 to be written as

$$\begin{aligned} p(\bar{n}) = & \frac{1}{Z} e^{-\beta[\psi(\bar{n}) + U(\bar{n})]} \\ & \times \sum_{m \geq n} \frac{\Lambda^m}{(m-n)!} \int \sum_{\mu \geq 0}^{m-n} \binom{m-n}{\mu} Q(\bar{n}; \bar{\mu}) e^{-\beta[\psi(\bar{m} - \bar{n}) + U(\bar{m} - \bar{n})]} d(\bar{m} - \bar{n}) \end{aligned} \tag{4.14}$$

Exchanging the summations over m and μ and expanding the binomial coefficient gives

$$\begin{aligned} p(\bar{n}) = & \frac{\Lambda^n}{Z} e^{-\beta[\psi(\bar{n}) + U(\bar{n})]} \\ & \times \sum_{\mu \geq 0} \frac{1}{\mu!} \sum_{m \geq n + \mu} \frac{\Lambda^{m-n}}{(m-n-\mu)!} \int Q(\bar{n}; \bar{\mu}) e^{-\beta[\psi(\bar{m} - \bar{n}) + U(\bar{m} - \bar{n})]} d(\bar{m} - \bar{n}). \end{aligned} \tag{4.15}$$

Substituting $\bar{m}' = \bar{m} - \bar{n}$ and integrating over the positions of the $\bar{m}' - \bar{\mu}$ particles gives

$$p(\bar{n}) = \Lambda^n e^{-\beta[\psi(\bar{n}) + U(\bar{n})]} \sum_{\mu \geq 0} \frac{1}{\mu!} \int Q(\bar{n}; \bar{\mu}) p(\bar{\mu}) d(\bar{\mu}). \tag{4.16}$$

Notice that this reduces for the one-body distribution function to

$$p(i) = \Lambda e^{-\beta[\psi(i)+v_1(i)]} \sum_{\mu\geq 0} \frac{1}{\mu!} \int Q(i;\bar{\mu}) p(\bar{\mu}) d(\bar{\mu}) \tag{4.17}$$

where $v_1(i)$ is the contribution of the one-body potential. This can be substituted into Equation 4.16 to find

$$p(\bar{n}) = e^{-\beta U'(\bar{n})} \prod_i^{\bar{n}} p(i) \frac{\sum_{\mu\geq 0} \frac{1}{\mu!} \int Q(\bar{n};\bar{\mu}) p(\bar{\mu}) d(\bar{\mu})}{\prod_i^{\bar{n}} \sum_{\mu\geq 0} \frac{1}{\mu!} \int Q(i;\bar{\mu}) p(\bar{\mu}) d(\bar{\mu})} \tag{4.18}$$

where $U'(\bar{n})$ is the same as $U(\bar{n})$, but excludes the one-body potential. Now consider a system with the same overall particle density where the imposed potential ψ and the one-body potential vanish, and where the boundary conditions do not break the symmetry of the remaining potentials; this will be called a uniform liquid of density p_0. For this system, Equation 4.18 becomes

$$p_0(\bar{n}) = e^{-\beta U'(\bar{n})} \prod_i^{\bar{n}} p_0 \frac{\sum_{\mu\geq 0} \frac{1}{\mu!} \int Q(\bar{n};\bar{\mu}) p_0(\bar{\mu}) d(\bar{\mu})}{\prod_i^{\bar{n}} \sum_{\mu\geq 0} \frac{1}{\mu!} \int Q(i;\bar{\mu}) p_0(\bar{\mu}) d(\bar{\mu})} \tag{4.19}$$

where symmetry requires the one-body distribution function to be equal to the overall particle density p_0. Dividing Equation 4.18 by Equation 4.19 gives

$$p(\bar{n}) = p_0(\bar{n}) \prod_i^{\bar{n}} \frac{p(i)}{p_0} \prod_i^{n} \frac{\sum_{\mu\geq 0} \frac{1}{\mu!} \int Q(i;\bar{\mu}) p_0(\bar{\mu}) d(\bar{\mu})}{\sum_{\mu\geq 0} \frac{1}{\mu!} \int Q(i;\bar{\mu}) p(\bar{\mu}) d(\bar{\mu})} \frac{\sum_{\mu\geq 0} \frac{1}{\mu!} \int Q(\bar{n};\bar{\mu}) p(\bar{\mu}) d(\bar{\mu})}{\sum_{\mu\geq 0} \frac{1}{\mu!} \int Q(\bar{n};\bar{\mu}) p_0(\bar{\mu}) d(\bar{\mu})}. \tag{4.20}$$

Although Equation 4.20 is exact, the distribution function $p(\bar{n})$ is coupled to the $p(\bar{\mu})$ for every μ by the fractional quantity in the innermost product. Assume that

these fractional quantities are all one. This is effectively the same as assuming that the ratio of the interaction of a cluster of n particles with the surrounding system to the interactions of n isolated particles with the surrounding system is the same in the fluid and in a uniform fluid with the same density. The n-body distribution function can now be approximated as

$$p(\bar{n}) = p_0(\bar{n}) \prod_i^{\bar{n}} \frac{p(i)}{p_0}. \tag{4.21}$$

Provided that the n-body distribution function for a uniform fluid of density p_0 is known, this provides a closure relation for any of the evolution equations in Equation 4.11. The systematic error introduced should be manageable as long as the average particle density is close to the overall particle density, as during solidification or crystallization reactions.

4.4. Distribution Functions in a Uniform Liquid

Consider using Equation A.1 from Appendix A to simulate the evolution of the one-body distribution function. If the three-body potential vanishes, the closure relation Equation 4.21 requires only the two-body distribution function for a uniform liquid. This can be found by iteratively applying Equation A.2 to a suitable initial condition until the function converges. If the one-body potential vanishes, the two-body potential depends on the relative coordinates $x_{ij} = x_j - x_i$ and $y_{ij} = y_j - y_i$ of the ith and jth particles, and the three-body distribution function is replaced by the Kirkwood superposition, Equation A.2 reduces to

$$\begin{aligned}\frac{\partial p_0(x_{12}, y_{12})}{\partial t} = \Gamma \sum_{i=1}^{2} \boldsymbol{\nabla}_i \cdot \Bigg[& k_B T \boldsymbol{\nabla}_i p_0(x_{12}, y_{12}) + \sum_{j \neq i}^{2} \boldsymbol{\nabla}_i v_2(x_{ij}, y_{ij}) p_0(x_{12}, y_{12}) \\ & + \frac{1}{p_0^3} \iint \boldsymbol{\nabla}_i v_2(x_{i3}, y_{i3}) p_0(x_{12}, y_{12}) p_0(x_{23}, y_{23}) p_0(x_{31}, y_{31}) dx_3 dy_3 \Bigg]\end{aligned} \tag{4.22}$$

Expanding Equation 4.22 and using the Fourier transforms from Appendix C gives

$$\begin{aligned}\frac{\partial p_0(x_{12},y_{12})}{\partial t} = \Gamma\Bigg[&k_BT\boldsymbol{\nabla}_2^2 p_0(x_{12},y_{12}) + k_BT\boldsymbol{\nabla}_1^2 p_0(x_{21},y_{21}) \\ &+ \boldsymbol{\nabla}_2^2 v_2(x_{12},y_{12})p_0(x_{12},y_{12}) + \boldsymbol{\nabla}_1^2 v_2(x_{21},y_{21})p_0(x_{21},y_{21}) \\ &+ \boldsymbol{\nabla}_2 v_2(x_{12},y_{12})\cdot\boldsymbol{\nabla}_2 p_0(x_{12},y_{12}) + \boldsymbol{\nabla}_1 v_2(x_{21},y_{21})\cdot\boldsymbol{\nabla}_1 p_0(x_{21},y_{21}) \\ &+ \frac{p_0(x_{12},y_{12})}{p_0^3}\iint \tilde{p}_0(u,v)\tilde{w}(u,v)\exp(2\pi i(ux_{12}+vy_{12}))dudv \\ &+ \frac{p_0(x_{21},y_{21})}{p_0^3}\iint \tilde{p}_0(u,v)\tilde{w}(u,v)\exp(2\pi i(ux_{21}+vy_{21}))dudv \\ &+ \frac{\boldsymbol{\nabla}_2 p_0(x_{12},y_{12})}{p_0^3}\cdot\iint \tilde{p}_0(u,v)\tilde{\boldsymbol{z}}(u,v)\exp(2\pi i(ux_{12}+vy_{12}))dudv \\ &+ \frac{\boldsymbol{\nabla}_1 p_0(x_{21},y_{21})}{p_0^3}\cdot\iint \tilde{p}_0(u,v)\tilde{\boldsymbol{z}}(u,v)\exp(2\pi i(ux_{21}+vy_{21}))dudv\Bigg]\end{aligned} \tag{4.23}$$

$w(x_{ij},y_{ij}) = \boldsymbol{\nabla}_j^2 v_2(x_{ij},y_{ij})p_0(x_{ij},y_{ij}) + \boldsymbol{\nabla}_j v_2(x_{ij},y_{ij})\cdot\boldsymbol{\nabla}_j p_0(x_{ij},y_{ij})$ and $\boldsymbol{z}(x_{ij},y_{ij}) = \boldsymbol{\nabla}_i v_2(x_{ij},y_{ij})p_0(x_{ij},y_{ij})$. Observing that $\boldsymbol{\nabla}_i f(x_{ij},y_{ij}) = -\boldsymbol{\nabla}_j f(x_{ij},y_{ij}) = \boldsymbol{\nabla}_i f(x_{ji},y_{ji})$ and $\boldsymbol{\nabla}_i^2 f(x_{ij},y_{ij}) = \boldsymbol{\nabla}_j^2 f(x_{ij},y_{ij}) = \boldsymbol{\nabla}_i^2 f(x_{ji},y_{ji})$ from Appendix B, the previous equation simplifies to

$$\begin{aligned}\frac{\partial p_0(x_{12},y_{12})}{\partial t} = 2\Gamma\Bigg[&k_BT\boldsymbol{\nabla}_2^2 p_0(x_{12},y_{12}) + \boldsymbol{\nabla}_2^2 v_2(x_{12},y_{12})p_0(x_{12},y_{12}) \\ &+ \boldsymbol{\nabla}_2 v_2(x_{12},y_{12})\cdot\boldsymbol{\nabla}_2 p_0(x_{12},y_{12}) \\ &+ \frac{p_0(x_{12},y_{12})}{p_0^3}\iint \tilde{p}_0(u,v)\tilde{w}(u,v)\exp(2\pi i(ux_{12}+vy_{12}))dudv \\ &+ \frac{\boldsymbol{\nabla}_2 p_0(x_{12},y_{12})}{p_0^3}\cdot\iint \tilde{p}_0(u,v)\tilde{\boldsymbol{z}}(u,v)\exp(2\pi i(ux_{12}+vy_{12}))dudv\Bigg]\end{aligned} \tag{4.24}$$

Since Equation 4.24 is a function of x_{12} and y_{12} alone, x_{12} and y_{12} can be replaced with x and y. Define $B(x,y)$ and $\boldsymbol{C}(x,y)$ as the results of the first and second integrals in the previous equation, respectively. The evolution equation for the two-body distribution

function for a uniform liquid is then

$$\frac{\partial p_0(x,y)}{\partial t} = 2\Gamma\left[k_B T \boldsymbol{\nabla}^2 p_0(x,y) + w(x,y) + \frac{p_0(x,y)}{p_0^3} B(x,y) + \frac{\boldsymbol{\nabla} p_0(x,y)}{p_0^3} \cdot \boldsymbol{C}(x,y)\right], \tag{4.25}$$

Iterative application of Equation 4.25 to a self-consistent state requires some initial condition. Given a two-body potential $v_2(x,y)$, a reasonable initial condition is

$$p_0(x,y) = \alpha e^{-\beta v_x(x,y)}. \tag{4.26}$$

We use Equation 4.25 to find the proper $p_0(x,y)$, and use this with Equation 4.21 to complete Equation A.1 and find an evolution equation for the one-body distribution function.

5. RESULTS AND DISCUSSION

5.1. Prospective

The stability and crystallization has been investigated by the method discussed in Chapter 4. This involves the evolution of the one-particle distribution function. The simulations can be used to visualize phase transition and solidification phenomena, and have several advantages over other available simulation methods with similar capabilities.

5.2. Simulation Setup and Procedures

As discussed in Chapter 4, the first objective is to find $p_0(x, y)$, the equilibrium 2-body distribution function for a uniform liquid for the given Morse potential. This is accomplished using Equation A.2 with the Kirkwood approximation to give an evolution equation for $p_0(x, y)$ in closed form. $p_0(x, y)$ is used in the evolution equation for the one-body distribution function in the next section.

The modeling process assumes that the first atom is fixed in the center of the box and effectively allows the remaining atoms to find their equilibration positions with respect to the central atom. More specifically, the two-body distribution function stipulates the expected atom density around a given atom in the uniform liquid. Note that this must be found in a self-consistent fashion, since every atom in the uniform liquid is indistinguishable. This is the source of the three-body term in Equation A.2 that is simplified by means of the Kirkwood approximation.

All simulations used in the $p_0(x, y)$ calculations consist of a square simulation box with 200 copper atoms for which $p_0(x, y)$ is calculated every time step. The simulation cell size varies depending on the temperature in accordance with the equilibrium volume per atom from the molecular dynamics simulations discussed in Chapter 3. The Morse

potential used was obtained from the literature [59,60], and is defined by the constants $\alpha = 1.3588$ Å^{-1}, $D = 0.3429$ eV and $r_0 = 2.866$ Å. The discontinuous derivations of the interaction energy around the origin were found to be a source of numerical instability. For this reason, we use a smoothed version of the potential. Within a distance of 1.7405 Å the Morse potential is replaced by a parabolic function with the same value and derivative at 1.7405 Å and a vanishing derivative at the origin. All numerical derivatives are calculated by finite differences with values in a uniform grid.

Values from the final condition of the molecular dynamics simulations which describe the thermodynamic state of the simulations (volume, density and temperature) are used to initialize the calculation of $p_0(x, y)$ with a normalized version of Equation 4.26. Simulations are run at constant temperature and constant volume (NVT ensemble).

The first simulation is run at 1350 K, the lower limit of the temperature range that brackets the solidification phase transition as found by MD simulation. The simulation cell is a square with edge length equal to $L = 13.2 \times 2.866$ Å and a planar density of $\rho = (200\text{atoms})/(13.2 \times 2.866\text{Å})^2 = 0.1397$ Å^{-2}, exactly the same as the converged planar density in MD at the specified temperature. $p_0(x, y)$ is explicitly evolved by Equation 4.25 with a time step of 10^{-6} s. Figure 5.1 and 5.2 show the gradual change of the two-body distribution function $p_0(x, y)$ around the origin of the simulation box as viewed along the x and z directions in increments of 50,000 simulation steps.

The perspective in Figure 5.2 helps to show the appearance of separate sharp rings around the particle in the center of the simulation cell. These rings correspond to the nearest neighbor shell of the central atom, the nearest neighbor shell of atoms in the first ring, etc. These appear as rings rather than points because there is nothing to break the circular symmetry in the uniform liquid. The absence of any atomic density in the center is a result of the repulsive part of the interatomic potential that lowers the probability of finding a particle in that region. The temperature on the figures has been reported in eV after multiplication by Boltzmann's constant.

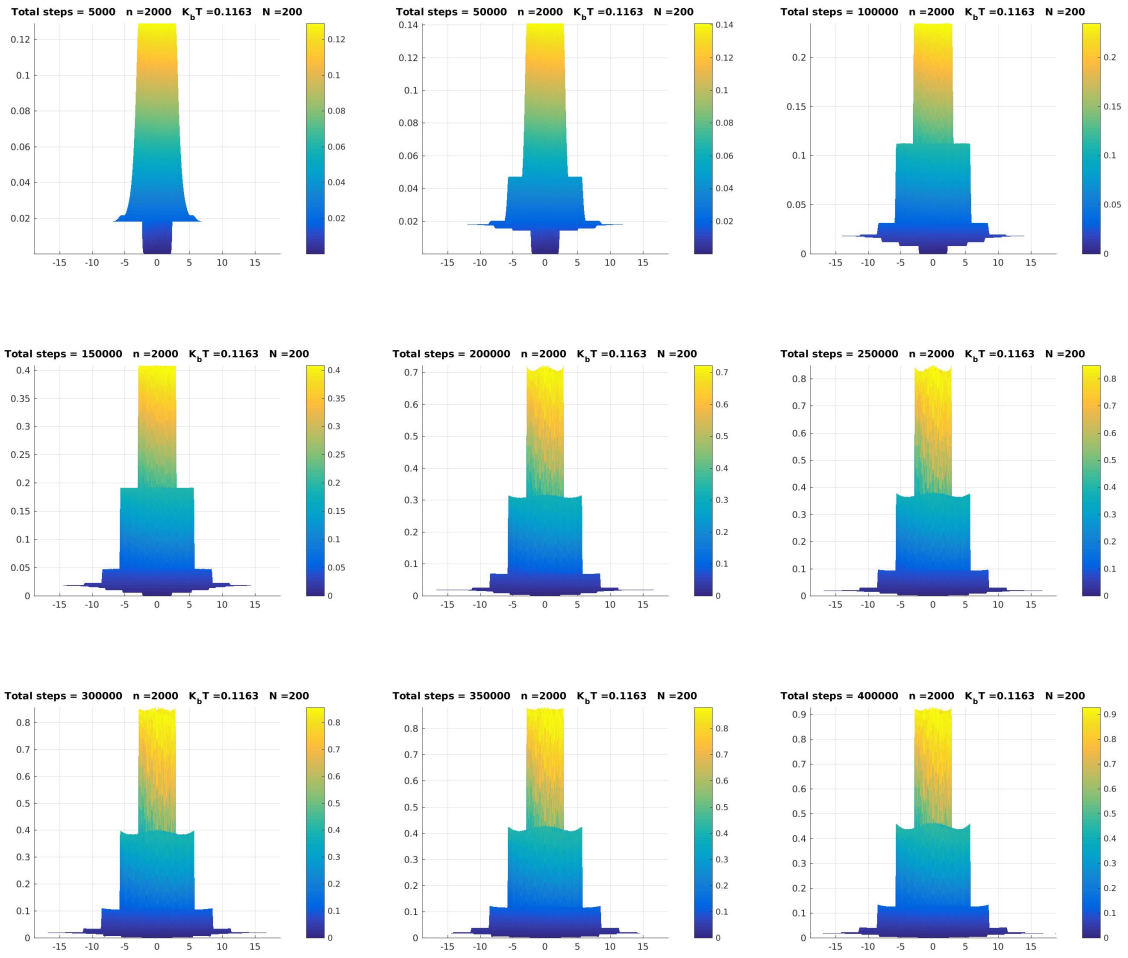

Figure 5.1. The gradual growth of the pair distribution function $p_0(x_{12}, y_{12})$ along the X direction .

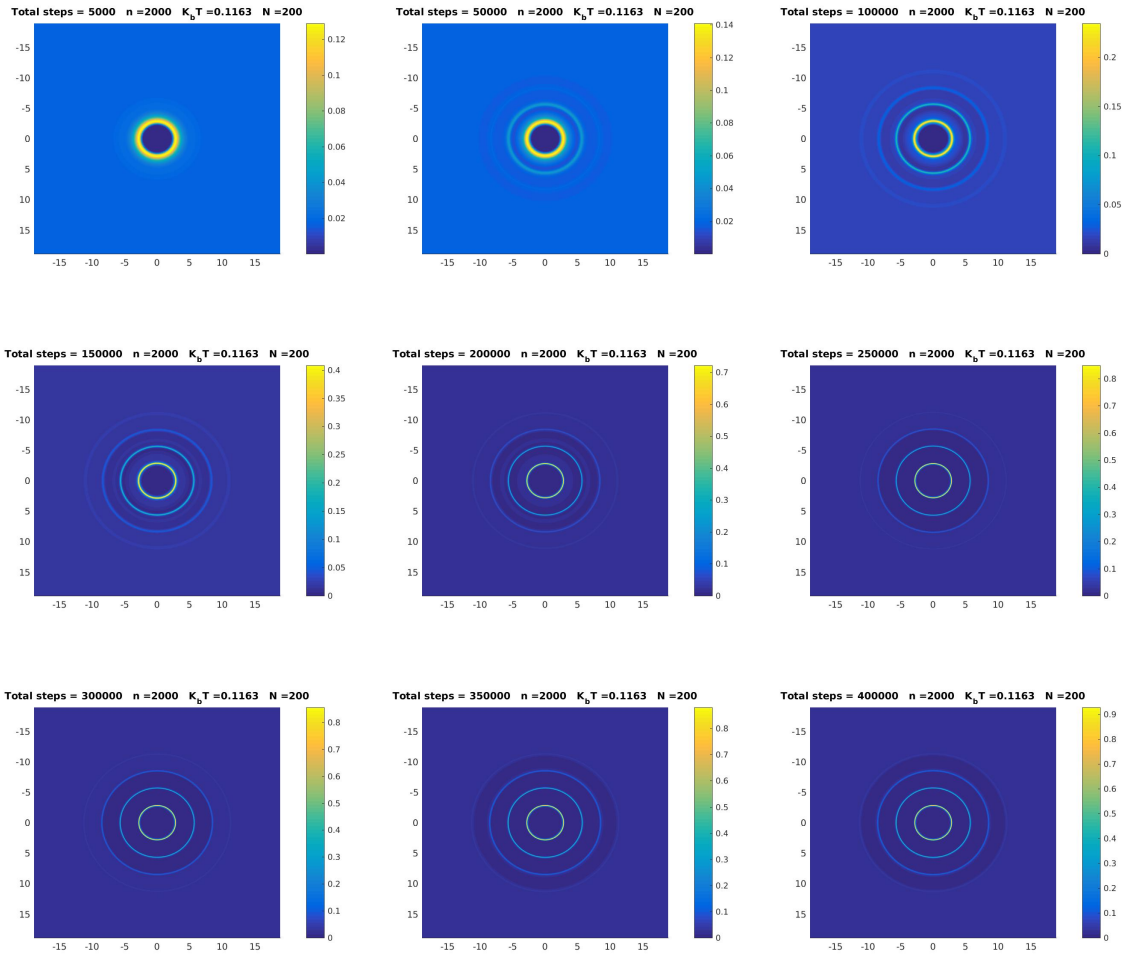

Figure 5.2. The gradual growth of the pair distribution function $p_0(x_{12}, y_{12})$ along the Z direction.

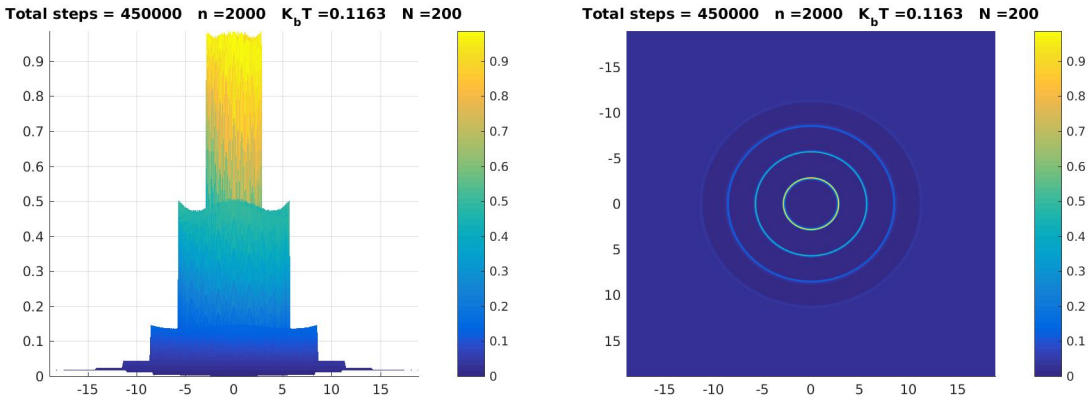

Figure 5.3. The final condition of the pair distribution function $p_0(x_{12}, y_{12})$ along the x and z directions.

The simulation appears to have converged after 450,000 time steps. The final $p_0(x_{12}, y_{12})$ is shown in Figure 5.3. The peaks no longer substantially change in hight after this point, and the rapid decay of the interatomic potential means that any rings outside the third will not meaningfully interact with the central atom. Beyond three or four times the equilibrium interatomic spacing the value remains the same as the background value of $N(N-1)/A$, where N is the number of atoms and A is the simulation cell area. The results from this section have been used in Section 6.5 to model the evolution of the one-body distribution function of copper just below the transition point.

5.3. Two-body Distribution Function at Different Temperatures

The two-body distribution function is expected to be a strong function of temperature, with the localization of the atomic density decreasing with temperature. Since the simulations are performed in the NPT ensemble, the volume is a function of temperature as well. Table 5.1 shows the area densities at various temperatures as determined by molecular dynamics. Figure 5.4 and 5.5 show the two-body distribution functions of copper atoms at the same temperatures as in Table 5.1. Observe from Figure 5.4 that the width of the rings around the central copper atom becomes wider at higher temperatures as compared to the thin and sharp rings at temperatures close to the

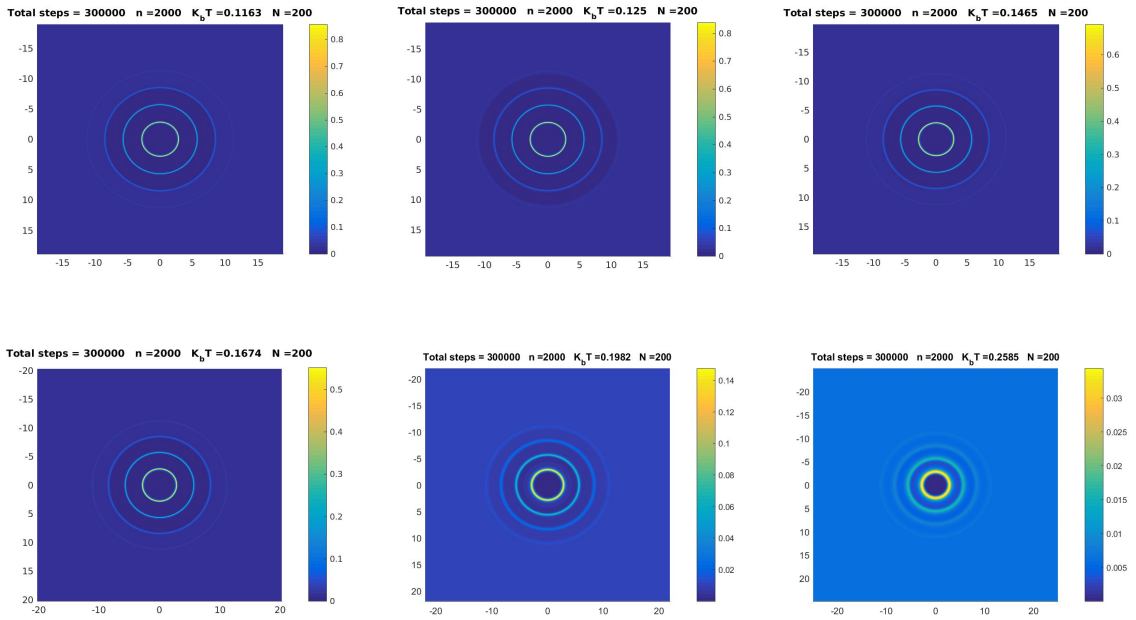

Figure 5.4. Different two-body distribution functions $p_0(x_{12}, y_{12})$ after 300,000 times steps of 10^{-6} s at six different temperatures along the z direction.

melting point. This is perhaps even more apparent from Figure 5.5 which reveals that the maximum height of $p_0(x, y)$ decreases from 0.8 to 0.03 as the temperature increases from 1350 K to 3000 K. This is entirely consistent with the existence of a solid with well-defined atomic locations at the lower end of the temperature range, and a liquid with random atomic displacements of increasing magnitude at the upper end of the range.

Table 5.1. Volume and density values reported from MD simulations of copper in two dimensions.

Temperature (K)	KT (eV)	Edge length (Å)	Area density (Å^{-1})
1350	0.1163	13.20×2.866	0.1397
1450	0.1250	13.52×2.866	0.1332
1700	0.1465	13.77×2.866	0.1330
2050	0.1674	14.14×2.866	0.1217
2350	0.1982	15.31×2.866	0.1038
3000	0.2585	17.40×2.866	0.0804

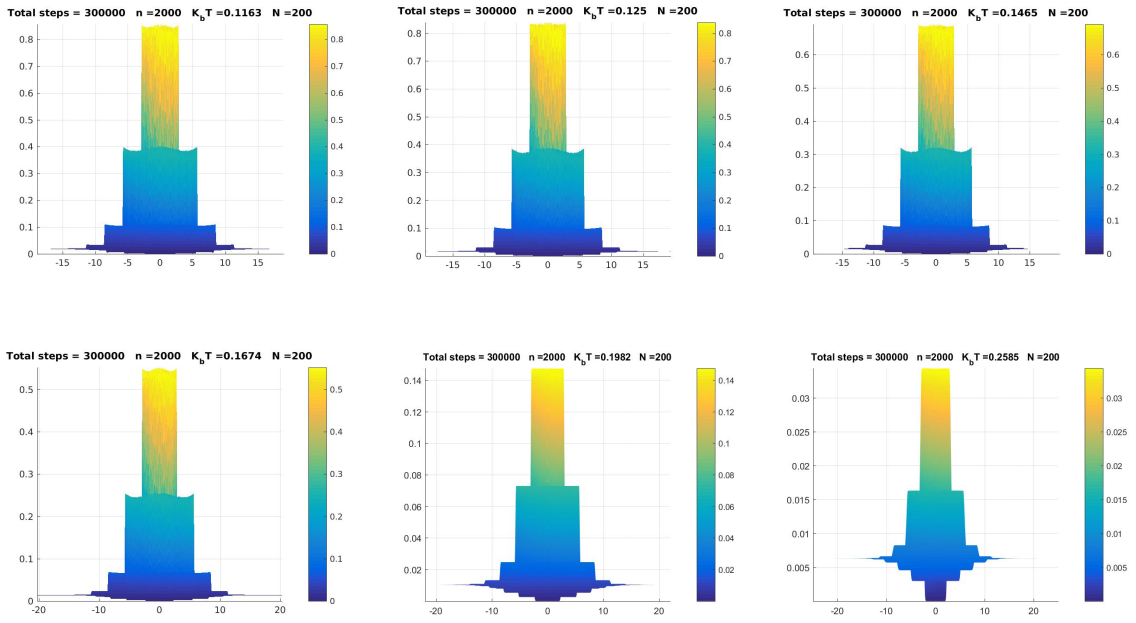

Figure 5.5. Different two-body distribution functions $p_0(x_{12}, y_{12})$ after 300,000 time steps of 10^{-6} s at six different temperatures along the X direction.

5.4. One-body Distribution Function at Melting Point of Copper

Whereas the results of the two-body distribution function were discussed in the previous two parts of this chapter, the one-body distribution function will be studied in this section. As mentioned at the end of Section 4.4, Equation 4.21 can be used to write Equation A.1 in terms of $p_0(x, y)$ and $p(1)$, giving a closed evolution equation for $p(1)$. The results are intended to show the solidification process of copper just below the melting point as reported by molecular dynamics simulations in Chapter 3.

Figure 5.3 depicts the two-body distribution function of the uniform liquid used in the current section. The one-body simulation uses exactly the same number of atoms, volume and temperature as the two-body simulation. A small perturbation is added to an initially uniform density. If the solid is the stable phase at this temperature, the perturbations should grow and the atoms localize. Perturbations are applied to three different locations inside the simulation cell. The simulation uses a time step of 10^{-5} s and the results are reported in Figure 5.6 in intervals of 500,000 time steps, up to a total of 4,500,000 time steps. Since the one-body distribution function is exactly an

atomic density, Figure 5.6 can be used to study the solidification of copper just below the melting point. The initial figures clearly show the increase of the magnitude of the perturbations applied with a wavelength equal to the equilibrium atomic spacing of the solid. Eventually, the perturbations interact with each other and the system boundaries to break the symmetry and specify atomic locations around at around 8,000,000 time steps. The evolution visibly continues even after this point, as the atoms relax further and the systems begins to crystallize. Further observe that the peaks in atomic density are not always symmetric. This indicates that the method is able to capture the preferential thermal vibrations of atoms into nearby regions where there is an excess of free volume.

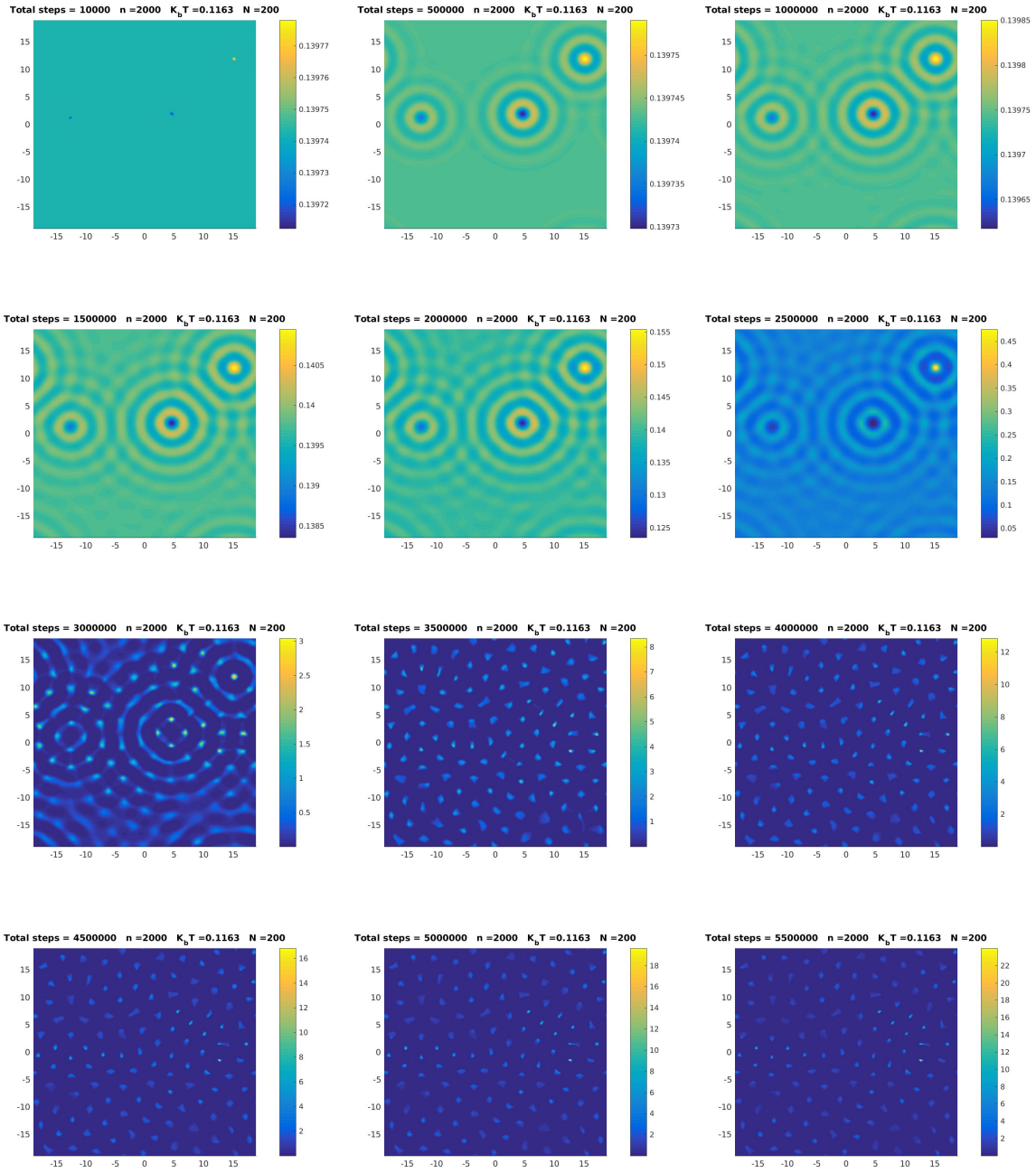

Figure 5.6. The evolution growth of the one-body distribution function $p(1)$ with increments of 500,000 time steps of 10^{-5} s between the plots.

6. CONCLUSION AND FUTURE WORKS

6.1. Conclusion

A new method was developed to model the behavior of atomic systems by using an accurate evolution equation with arbitrary interatomic potential on diffusive time scales. According to the attained results, we can claim that this model is able to study the solidification of a solid and show the phase transition at the melting point. The behavior of two-body distribution clearly indicates a strong temperature function which was an expected result due to the localization of the atomic density. The formulation of current method provides the one-body distribution function in a closed form with explicit interatomic potential. By obtaining the results from the one-body distribution, we are able to determine and specify the atomic locations and this atomic density could be used to study the solidification. The results of this thesis indicate that we can study the crystalline formation with longer time scale compared with the preferred method in the literature (molecular dynamics).

6.2. Future Works

There are several directions that this work could be extended without further theoretical development. First, the simulation results in Section 5.4 could be extended to longer times to follow the nucleation and growth of a crystal from the initially disordered solid. Nucleation phenomena occur on a time scale that is significantly longer than can be accessed by MD (the method preferred in the literature), and this presents an opportunity to learn more about the energetics and kinetics of crystallite formation. Second, the enthalpy of the system could be calculated from the interatomic potential, the two-body distribution function for a uniform liquid, and the one-body distribution function. Provided the one-body distribution function is already localized, this could be used to validate the method by comparing the enthalpy with the time-averaged enthalpy of a MD simulation with the same number of atoms, volume, temperature, and atomic configuration. Third, the time-averaged positions of the atoms in the above MD

simulation could be compared with the shape of the peaks in atomic density in Figure 5.6 to verify that the method effectively integrates the atomic motion over shorter time scales.

Once the initial validation is completed, similar simulations could be performed at other pressures and temperatures. The qualitative behavior of the one-body distribution function is expected to be a strong function of pressure and temperature, with the crystallization of the solid phase kinetically obstructed at sufficiently low temperatures and high pressures and the one-body distribution function developing stability with respect to perturbations at sufficiently high temperatures and low pressures. Since this latter behavior would effectively indicate the thermodynamic favorability of the liquid phase over the solid phase, the method could be used to construct a PT phase diagram for the given interatomic potential. This could then be validated by the PT diagram constructed from the corresponding MD simulations, with the understanding that crystallization occurs on a prohibitively long time scale for MD and all simulations would need to begin in the solid phase rather than the liquid phase.

The effect of the Kirkwood approximation on the calculation of the two-body distribution function and Equation 4.21 on the calculation of the one-body distribution function is not yet known. One possible result could be that the PT diagrams constructed above do not agree, suggesting a systematic error in the equations developed in Chapter 4. The simplest way to improve the accuracy would be to use Equations A.2 and A.3 and the Fisher and Kopeliovich approximation [62] to calculate the two- and three-body distribution functions of the uniform liquid. This would give a (presumably more accurate) two-body distribution function of the uniform liquid that could then be used with Equations A.1 and 4.21 to find a different evolution equation for the one-body distribution function. Alternatively, Equation 4.21 could be modified to include functional derivatives of $p_0(\bar{n})$ with respect to $p(i)$, as for the local-density approximation in DFT. It is not yet known if such a procedure is necessary, would improve the accuracy of the calculated PT diagram, or would even be computationally feasible.

Provided the method is validated in two dimensions, the next step would be to extend the method to three dimensions. This would not require substantial algorithmic changes, but would involve rewriting the existing code in a compiled language more suited to demanding numerical work (e.g., C++). The benefits would include the ability to model other crystal structures, to study more diverse kinetic phenomena including diffusion and dislocation climb, and possibly even to connect the simulation results with experiments. While a comparison with experiments would be complicated by the fact that the interatomic potential for, e.g., pure copper, is not precisely known, the true purpose of simulations is to be informed by and guide experiments. Establishing a connection with experiments as early as possible would therefore be invaluable for the further development of the model.

Eventually, the theory could be developed further to allow for three body interactions, allowing the simulation of covalently bonded materials, or three atomic types with three pairwise interactions. While incremental from the standpoint of the theory, these would significantly increase the complexity of the computational implementation. Nevertheless, these extensions would eventually be necessary for the method to achieve widespread utility and acceptance.

REFERENCES

1. Evans, R., "The nature of the liquid-vapour interface and other topics in the statistical mechanics of non-uniform, classical fluids", *Advances in Physics*, Vol. 28, No. 2, pp. 143–200, 1979.

2. Marconi, U. M. B. and P. Tarazona, "Dynamic density functional theory of fluids", *The Journal of Chemical Physics*, Vol. 110, No. 16, pp. 8032–8044, 1999.

3. Keller, J. and J. L. Gázquez, "Density functional theory", *Lecture Notes in Physics, Berlin Springer Verlag*, Vol. 187, 1983.

4. Archer, A. J. and R. Evans, "Dynamical density functional theory and its application to spinodal decomposition", *The Journal of chemical physics*, Vol. 121, No. 9, pp. 4246–4254, 2004.

5. Archer, A. J. and M. Rauscher, "Dynamical density functional theory for interacting Brownian particles: stochastic or deterministic?", *Journal of Physics A: Mathematical and General*, Vol. 37, No. 40, p. 9325, 2004.

6. Hansen, J.-P. and I. R. McDonald, *Theory of simple liquids*, Elsevier, 1990.

7. Parr, R. G., "Density functional theory of atoms and molecules", *Horizons of Quantum Chemistry*, pp. 5–15, Springer, 1980.

8. Archer, A. J., "Dynamical density functional theory for dense atomic liquids", *Journal of Physics: Condensed Matter*, Vol. 18, No. 24, p. 5617, 2006.

9. Archer, A. J., "Dynamical density functional theory: binary phase-separating colloidal fluid in a cavity", *Journal of Physics: Condensed Matter*, Vol. 17, No. 10, p. 1405, 2005.

10. Evans, R., "Density functionals in the theory of nonuniform fluids", *Fundamentals of Inhomogeneous Fluids*, Vol. 1, pp. 85–176, 1992.

11. Dean, D. S., "Langevin equation for the density of a system of interacting Langevin processes", *Journal of Physics A: Mathematical and General*, Vol. 29, No. 24, p. L613, 1996.

12. Kawasaki, K., "Stochastic model of slow dynamics in supercooled liquids and dense colloidal suspensions", *Physica A: Statistical Mechanics and its Applications*, Vol. 208, No. 1, pp. 35–64, 1994.

13. Kawasaki, K. and S. Miyazima, "Path integral formulation of dynamical density functional equation for dense fluids", *Zeitschrift für Physik B Condensed Matter*, Vol. 103, No. 3, pp. 423–431, 1997.

14. Marconi, U. M. B. and P. Tarazona, "Dynamic density functional theory of fluids", *Journal of Physics: Condensed Matter*, Vol. 12, No. 8A, p. A413, 2000.

15. Dieterich, W., H. Frisch and A. Majhofer, "Nonlinear diffusion and density functional theory", *Zeitschrift für Physik B Condensed Matter*, Vol. 78, No. 2, pp. 317–323, 1990.

16. Evans, R., "The nature of the liquid-vapour interface and other topics in the statistical mechanics of non-uniform, classical fluids", *Advances in Physics*, Vol. 28, No. 2, pp. 143–200, 1979.

17. Stopper, D., R. Roth and H. Hansen-Goos, "Communication: Dynamical density functional theory for dense suspensions of colloidal hard spheres", *The Journal of chemical physics*, Vol. 143, No. 18, p. 181105, 2015.

18. Stopper, D., K. Marolt, R. Roth and H. Hansen-Goos, "Modeling diffusion in colloidal suspensions by dynamical density functional theory using fundamental measure theory of hard spheres", *Physical Review E*, Vol. 92, No. 2, p. 022151,

2015.

19. Malijevskỳ, A. and A. J. Archer, "Sedimentation of a two-dimensional colloidal mixture exhibiting liquid-liquid and gas-liquid phase separation: A dynamical density functional theory study", *The Journal of chemical physics*, Vol. 139, No. 14, p. 144901, 2013.

20. van Teeffelen, S., C. V. Achim and H. Löwen, "Vacancy diffusion in colloidal crystals as determined by dynamical density-functional theory and the phase-field-crystal model", *Physical Review E*, Vol. 87, No. 2, p. 022306, 2013.

21. Moelans, N., B. Blanpain and P. Wollants, "An introduction to phase-field modeling of microstructure evolution", *Calphad*, Vol. 32, No. 2, pp. 268–294, 2008.

22. Elder, K., M. Katakowski, M. Haataja and M. Grant, "Modeling elasticity in crystal growth", *Physical review letters*, Vol. 88, No. 24, p. 245701, 2002.

23. Elder, K. and M. Grant, "Modeling elastic and plastic deformations in nonequilibrium processing using phase field crystals", *Physical Review E*, Vol. 70, No. 5, p. 051605, 2004.

24. Elder, K., N. Provatas, J. Berry, P. Stefanovic and M. Grant, "Phase-field crystal modeling and classical density functional theory of freezing", *Physical Review B*, Vol. 75, No. 6, p. 064107, 2007.

25. Oettel, M., S. Dorosz, M. Berghoff, B. Nestler and T. Schilling, "Description of hard-sphere crystals and crystal-fluid interfaces: A comparison between density functional approaches and a phase-field crystal model", *Physical review E*, Vol. 86, No. 2, p. 021404, 2012.

26. Emmerich, H., H. Löwen, R. Wittkowski, T. Gruhn, G. I. Tóth, G. Tegze and L. Gránásy, "Phase-field-crystal models for condensed matter dynamics on atomic length and diffusive time scales: an overview", *Advances in Physics*, Vol. 61, No. 6,

pp. 665–743, 2012.

27. van Teeffelen, S., R. Backofen, A. Voigt and H. Löwen, "Derivation of the phase-field-crystal model for colloidal solidification", *Physical Review E*, Vol. 79, No. 5, p. 051404, 2009.

28. Pisutha-Arnond, N., V. Chan, K. Elder and K. Thornton, "Calculations of isothermal elastic constants in the phase-field crystal model", *Physical Review B*, Vol. 87, No. 1, p. 014103, 2013.

29. Burke, K., "Perspective on density functional theory", *The Journal of chemical physics*, Vol. 136, No. 15, p. 150901, 2012.

30. Greenwood, M., N. Provatas and J. Rottler, "Free energy functionals for efficient phase field crystal modeling of structural phase transformations", *Physical review letters*, Vol. 105, No. 4, p. 045702, 2010.

31. Ofori-Opoku, N., V. Fallah, M. Greenwood, S. Esmaeili and N. Provatas, "Multicomponent phase-field crystal model for structural transformations in metal alloys", *Physical Review B*, Vol. 87, No. 13, p. 134105, 2013.

32. Berry, J., K. Elder and M. Grant, "Melting at dislocations and grain boundaries: A phase field crystal study", *Physical Review B*, Vol. 77, No. 22, p. 224114, 2008.

33. Provatas, N., N. Goldenfeld and J. Dantzig, "Adaptive mesh refinement computation of solidification microstructures using dynamic data structures", *Journal of computational physics*, Vol. 148, No. 1, pp. 265–290, 1999.

34. Swift, J. and P. C. Hohenberg, "Hydrodynamic fluctuations at the convective instability", *Physical Review A*, Vol. 15, No. 1, p. 319, 1977.

35. Jin, Y. M. and A. G. Khachaturyan, "Atomic density function theory and modeling of microstructure evolution at the atomic scale", *Journal of applied physics*, Vol.

100, No. 1, p. 013519, 2006.

36. Asadi, E. and M. A. Zaeem, "A review of quantitative phase-field crystal modeling of solid–liquid structures", *JOM*, Vol. 67, No. 1, pp. 186–201, 2015.

37. Provatas, N., N. Goldenfeld, J. Dantzig, J. C. LaCombe, A. Lupulescu, M. B. Koss, M. E. Glicksman and R. Almgren, "Crossover scaling in dendritic evolution at low undercooling", *Physical Review Letters*, Vol. 82, No. 22, p. 4496, 1999.

38. Emdadi, A., M. A. Zaeem and E. Asadi, "Revisiting phase diagrams of two-mode phase-field crystal models", *Computational Materials Science*, Vol. 123, pp. 139–147, 2016.

39. Berry, J., M. Grant and K. Elder, "Diffusive atomistic dynamics of edge dislocations in two dimensions", *Physical Review E*, Vol. 73, No. 3, p. 031609, 2006.

40. Jaatinen, A., C. Achim, K. Elder and T. Ala-Nissila, "Thermodynamics of bcc metals in phase-field-crystal models", *Physical review E*, Vol. 80, No. 3, p. 031602, 2009.

41. Emmerich, H., H. Löwen, R. Wittkowski, T. Gruhn, G. I. Tóth, G. Tegze and L. Gránásy, "Phase-field-crystal models for condensed matter dynamics on atomic length and diffusive time scales: an overview", *Advances in Physics*, Vol. 61, No. 6, pp. 665–743, 2012.

42. Landry, E. S., *Thermal transport by phonons across semiconductor interfaces, thin films, and superlattices*, Ph.D. Thesis, Carnegie Mellon University, 2009.

43. McGaughey, A. J. and M. Kaviany, "Phonon transport in molecular dynamics simulations: formulation and thermal conductivity prediction", *Advances in Heat Transfer*, Vol. 39, pp. 169–255, 2006.

44. Alder, B. and T. Wainwright, "Molecular dynamics by electronic computers",

Transport processes in statistical mechanics, pp. 97–131, 1958.

45. Karplus, M. and J. A. McCammon, "Molecular dynamics simulations of biomolecules", *Nature Structural & Molecular Biology*, Vol. 9, No. 9, pp. 646–652, 2002.

46. Landry, E., S. Mikkilineni, M. Paharia and A. McGaughey, "Droplet evaporation: A molecular dynamics investigation", *Journal of Applied Physics*, Vol. 102, No. 12, p. 124301, 2007.

47. Patodia, S., A. Bagaria and D. Chopra, "Molecular Dynamics Simulation of Proteins: A Brief Overview", *Journal of Physical Chemistry & Biophysics*, Vol. 4, No. 6, p. 1, 2014.

48. Zhang, J., F. Xu, Y. Hong, Q. Xiong and J. Pan, "A comprehensive review on the molecular dynamics simulation of the novel thermal properties of graphene", *RSC Advances*, Vol. 5, No. 109, pp. 89415–89426, 2015.

49. Oluwajobi, A. and X. Chen, "The effect of interatomic potentials on the molecular dynamics simulation of nanometric machining", *International Journal of Automation and Computing*, Vol. 8, No. 3, pp. 326–332, 2011.

50. Yip, S., *Handbook of materials modeling*, Springer Science & Business Media, 2007.

51. Allen, M. P. *et al.*, "Introduction to molecular dynamics simulation", *Computational soft matter: from synthetic polymers to proteins*, Vol. 23, pp. 1–28, 2004.

52. Waheed, Q. and O. Edholm, "Quantum corrections to classical molecular dynamics simulations of water and ice", *Journal of chemical theory and computation*, Vol. 7, No. 9, pp. 2903–2909, 2011.

53. Hill, T. L., *Statistical mechanics: principles and selected applications*, Courier Corporation, 2013.

54. McQuarrie, D., "Statistical Mechanics. 2000", *Sausalito, California: University Science Books*, Vol. 12, p. 641, 2000.

55. Rice, O. K. *et al.*, *Statistical mechanics, thermodynamics and kinetics*, WH Freeman San Francisco, 1967.

56. Rudzinski, J. F. and W. Noid, "A generalized-Yvon-Born-Green method for coarse-grained modeling", *The European Physical Journal Special Topics*, Vol. 224, No. 12, pp. 2193–2216, 2015.

57. Das, S. P., *Statistical physics of liquids at freezing and beyond*, Cambridge University Press, 2011.

58. Plimpton, S., "Fast parallel algorithms for short-range molecular dynamics", *Journal of computational physics*, Vol. 117, No. 1, pp. 1–19, 1995.

59. Girifalco, L. A. and V. G. Weizer, "Application of the Morse potential function to cubic metals", *Physical Review*, Vol. 114, No. 3, p. 687, 1959.

60. Singh, J. K., J. Adhikari and S. K. Kwak, "Vapor–liquid phase coexistence curves for Morse fluids", *Fluid phase equilibria*, Vol. 248, No. 1, pp. 1–6, 2006.

61. Meeron, E., "Nodal expansions. Distribution functions, potentials of average force, and the Kirkwood superposition approximation", *Physics of Fluids (1958-1988)*, Vol. 1, No. 2, pp. 139–149, 1958.

62. Fisher, I., "Present state of the theory of liquids", *Physics-Uspekhi*, Vol. 5, No. 2, pp. 239–250, 1962.

APPENDIX A: YBG EQUATIONS FOR THREE-BODY POTENTIALS

As explained in Section 4.2 , Equation 4.11 gives the time derivative of the n-body distribution function assuming a potential that depends only on the positions of the particles. If the potential contains one-, two-, and three-body components, and a dependence on the position of the ith particle is indicated by the integer i, the time derivative of the one-body distribution function is

$$\frac{\partial p(1)}{\partial t} = \Gamma \boldsymbol{\nabla}_1 \cdot \Big[k_B T \boldsymbol{\nabla}_1 p(1) + \boldsymbol{\nabla}_1 v_1(1) p(1) + \int \boldsymbol{\nabla}_1 v_2(1,2) p(1,2) d(2) + \frac{1}{2} \iint \boldsymbol{\nabla}_1 v_3(1,2,3) p(1,2,3) d(2,3) \Big]. \tag{A.1}$$

The time derivative of the two-body distribution function is

$$\begin{aligned} \frac{\partial p(1,2)}{\partial t} = \Gamma \sum_{i=1}^{2} \boldsymbol{\nabla}_i \cdot \Big[& k_B T \boldsymbol{\nabla}_i p(1,2) + \boldsymbol{\nabla}_i v_1(i) p(1,2) \\ & + \sum_{j \neq i}^{2} \boldsymbol{\nabla}_i v_2(i,j) p(1,2) + \int \boldsymbol{\nabla}_i v_2(i,3) p(1,2,3) d(3) \\ & + \sum_{j \neq i}^{2} \int \boldsymbol{\nabla}_i v_3(i,j,3) p(1,2,3) d(3) \\ & + \frac{1}{2} \iint \boldsymbol{\nabla}_i v_3(i,3,4) p(1,2,3,4) d(3,4) \Big]. \end{aligned} \tag{A.2}$$

The time derivative of the three-body distribution function is

$$\frac{\partial p(1,2,3)}{\partial t} = \Gamma \sum_{i=1}^{3} \boldsymbol{\nabla}_i \cdot \Bigg[k_B T \boldsymbol{\nabla}_i p(1,2,3) + \boldsymbol{\nabla}_i v_1(i) p(1,2,3) + \sum_{j \neq i}^{3} \boldsymbol{\nabla}_i v_2(i,j) p(1,2,3) + \frac{1}{2} \sum_{j \neq i}^{3} \sum_{k \neq i,j}^{3} \boldsymbol{\nabla}_i v_3(i,j,k) p(1,2,3) + \int \boldsymbol{\nabla}_i v_2(i,4) p(1,2,3,4) d(4) + \sum_{j \neq i}^{3} \int \boldsymbol{\nabla}_i v_3(i,j,4) p(1,2,3,4) d(4) + \iint \boldsymbol{\nabla}_i v_3(i,4,5) p(1,2,3,4,5) d(4,5) \Bigg]. \tag{A.3}$$

APPENDIX B: LAPLACIAN AND GRADIENT RELATIONS

Suppose that a function f depends only on the distance separating particles 1 and 2. This can be written as $f(x_{12}, y_{12})$ where, e.g., $x_{12} = x_2 - x_1$. Since f is a function of distance only, the symmetry $f(x_{12}, y_{12}) = f(x_{21}, y_{21})$ holds. The following equalities hold by the chain rule:

$$\begin{aligned}\boldsymbol{\nabla}_1 f(x_{12}, y_{12}) &= \hat{\mathbf{x}}\frac{\partial x_{12}}{\partial x_1}\frac{\partial f(x_{12}, y_{12})}{\partial x_{12}} + \hat{\mathbf{y}}\frac{\partial y_{12}}{\partial y_1}\frac{\partial f(x_{12}, y_{12})}{\partial y_{12}} \\ &= -\hat{\mathbf{x}}\frac{\partial f(x_{12}, y_{12})}{\partial x_{12}} - \hat{\mathbf{y}}\frac{\partial f(x_{12}, y_{12})}{\partial y_{12}} \end{aligned} \tag{B.1}$$

$$\begin{aligned}\boldsymbol{\nabla}_2 f(x_{12}, y_{12}) &= \hat{\mathbf{x}}\frac{\partial x_{12}}{\partial x_2}\frac{\partial f(x_{12}, y_{12})}{\partial x_{12}} + \hat{\mathbf{y}}\frac{\partial y_{12}}{\partial y_2}\frac{\partial f(x_{12}, y_{12})}{\partial y_{12}} \\ &= \hat{\mathbf{x}}\frac{\partial f(x_{12}, y_{12})}{\partial x_{12}} + \hat{\mathbf{y}}\frac{\partial f(x_{12}, y_{12})}{\partial y_{12}} \end{aligned} \tag{B.2}$$

Similar reasoning and the symmetry $f(x_{12}, y_{12}) = f(x_{21}, y_{21})$ gives:

$$\begin{aligned}\boldsymbol{\nabla}_2 f(x_{21}, y_{21}) &= \hat{\mathbf{x}}\frac{\partial x_{21}}{\partial x_2}\frac{\partial f(x_{21}, y_{21})}{\partial x_{21}} + \hat{\mathbf{y}}\frac{\partial y_{21}}{\partial y_2}\frac{\partial f(x_{21}, y_{21})}{\partial y_{21}} \\ &= -\hat{\mathbf{x}}\frac{\partial f(x_{21}, y_{21})}{\partial x_{21}} - \hat{\mathbf{y}}\frac{\partial f(x_{21}, y_{21})}{\partial y_{21}} \\ &= \hat{\mathbf{x}}\frac{\partial f(x_{12}, y_{12})}{\partial x_{12}} + \hat{\mathbf{y}}\frac{\partial f(x_{12}, y_{12})}{\partial y_{12}} \end{aligned} \tag{B.3}$$

$$\begin{aligned}\boldsymbol{\nabla}_1 f(x_{21}, y_{21}) &= \hat{\mathbf{x}}\frac{\partial x_{21}}{\partial x_1}\frac{\partial f(x_{21}, y_{21})}{\partial x_{21}} + \hat{\mathbf{y}}\frac{\partial y_{21}}{\partial y_1}\frac{\partial f(x_{21}, y_{21})}{\partial y_{21}} \\ &= \hat{\mathbf{x}}\frac{\partial f(x_{21}, y_{21})}{\partial x_{21}} + \hat{\mathbf{y}}\frac{\partial f(x_{21}, y_{21})}{\partial y_{21}} \\ &= -\hat{\mathbf{x}}\frac{\partial f(x_{12}, y_{12})}{\partial x_{12}} - \hat{\mathbf{y}}\frac{\partial f(x_{12}, y_{12})}{\partial y_{12}} \end{aligned} \tag{B.4}$$

This means that for this function, the following symmetries hold:

$$-\boldsymbol{\nabla}_1 f(x_{21}, y_{21}) = \boldsymbol{\nabla}_2 f(x_{21}, y_{21}) = -\boldsymbol{\nabla}_1 f(x_{12}, y_{12}) = \boldsymbol{\nabla}_2 f(x_{12}, y_{12}) \tag{B.5}$$

The corresponding symmetries for the Laplacian are:

$$\boldsymbol{\nabla}_1^2 f(x_{21}, y_{21}) = \boldsymbol{\nabla}_2^2 f(x_{21}, y_{21}) = \boldsymbol{\nabla}_1^2 f(x_{12}, y_{12}) = \boldsymbol{\nabla}_2^2 f(x_{12}, y_{12}) \tag{B.6}$$

That is, all versions of the Laplacian are the same.

APPENDIX C: FOURIER TRANSFORMS

Suppose that a function $f(x)$ depends on $-\infty < x < +\infty$. The Fourier transform $\tilde{f}(w)$ of $f(x)$ is given by

$$\tilde{f}(w) = \int_{-\infty}^{+\infty} f(x) e^{-2\pi i x w}\, dx. \tag{C.1}$$

The inverse of this operation is

$$f(x) = \int_{-\infty}^{+\infty} \tilde{f}(w) e^{2\pi i x w}\, dw. \tag{C.2}$$

The Fourier transform can be generalized to higher dimensions. For example suppose that a function $f(x, y)$ depends on $-\infty < x < +\infty$ and $-\infty < y < +\infty$. The Fourier transform $\tilde{f}(u, v)$ of $f(x, y)$ is

$$\tilde{f}(u, v) = \int_{-\infty}^{+\infty} \int_{-\infty}^{+\infty} f(x, y) e^{-2i\pi(ux+vy)}\, dxdy. \tag{C.3}$$

The inverse of this operation is

$$f(x, y) = \int_{-\infty}^{+\infty} \int_{-\infty}^{+\infty} \tilde{f}(u, v) e^{2i\pi(ux+vy)}\, dudv \tag{C.4}$$

APPENDIX D: SIMULATION CODES

MATLAB codes for the calculation of two-body and one-body distribution functions are reported in this section.

D.1. Two-body Distribution

```
% Evoluation equation for the two-body distirbution function
% Constants
G = 1; % Gama
n = 2000;      % number of grid points along the edge
L = 13.52 * 2.866;      % length of simulation cell edge
A = L.^2;    % Area of the system
N = 200;     % number of particles
KbT = 0.1163;      %2050 K
Beta = 1/KbT; % Boltzmann constant k_b = 8.61733e-5 [eV/K]
step = 1e-6;    % length of time step
total_step = 450000; % total number of steps
ploting_step = 5000; % every ploting step it plots p0_12
% Morse potential constants
epsilon = 0.3492;
alpha = 1.357;
r_e = 2.866;
constantP = N/(L^2);
delta = L/n; % the spacing of the grid
% Definition of Particles:
% First Particle
x1 = 0;
y1 = 0;
% Second Particle
x2 = linspace(-L/2,L/2,n+1)' * ones(1,n+1);
```

```
25 x2 = x2(1:end-1, 1:end-1);
26 y2 = ones(1,n+1)' * linspace(-L/2,L/2,n+1);
27 y2 = y2(1:end-1, 1:end-1);
28 Filter = sqrt(x2.^2 + y2.^2) < 3.5 .* r_e;
29 % evaluation of distance
30 distance12 = sqrt ( x2.^2 + y2.^2);
31 % Definition of Potential:
32 % Morse Potential
33 v2_12 = Morse( epsilon, alpha , r_e, distance12 , n );
34 % Third Particle
35 x3 = x2;
36 y3 = y2;
37 % evaluation of distance & Potential v_2
38 distance13 = distance12;
39 v2_13 = v2_12;
40 % SECOND PARTICLE      1---2
41 lap_v2_12 = laplacian3( v2_12, delta);
42 grad_v2_12_x  = nablax(v2_12,delta);
43 grad_v2_12_y  = nablay(v2_12,delta);
44 % THIRD PARTICLE       1---3
45 lap_v2_13 = lap_v2_12;
46 grad_v2_13_x = grad_v2_12_x;
47 grad_v2_13_y = grad_v2_12_y;
48 % SECOND and THIRD     2---3
49 lap_v2_23 = circshift(lap_v2_12,[n/2 , n/2]);
50 grad_v2_23_x = circshift(grad_v2_12_x,[n/2 , n/2]);
51 grad_v2_23_y = circshift(grad_v2_12_y,[n/2 , n/2]);
52 diffx = x2(2,1)- x2(1,1);
53 diffy = y2(1,2)- y2(1,1);
54 dA = diffx * diffy;
55 % values relates to P_0 that do not change as it iterates:
```

```
% SECOND PARTICLE      1---2
p0_12 = exp(-Beta.* v2_12);
p0_12 = p0_12 * (N * (N-1) / A) / (sum(sum(p0_12)) * dA);
val = zeros(total_step,1);
var_plot = zeros(n,n,total_step/ploting_step);
max_delta = 0;
abs_delta = [];
iii =1;
start=1;
for s = start:total_step
    lap_p0_12 = laplacian3(p0_12,delta);
    grad_p0_12_x = nablax(p0_12,delta);
    grad_p0_12_y = nablay(p0_12,delta);
    % THIRD PARTICLE      1---3
    p0_13 = p0_12;
    grad_p0_13_x = grad_p0_12_x;
    grad_p0_13_y = grad_p0_12_y;
    % Second and Third    2---3
    p0_23 = circshift(p0_12,[n/2, n/2]);
    grad_p0_23_x = circshift(grad_p0_12_x,[n/2, n/2]);
    grad_p0_23_y = circshift(grad_p0_12_y,[n/2, n/2]);
    % Evaluation of formula :
    %%% 1st term
    first = KbT .* lap_p0_12;
    %%% 2nd term
    second = lap_v2_12 .* p0_12 + ...
    grad_p0_12_x.* grad_v2_12_x+ grad_p0_12_y.* grad_v2_12_y;
    %%% 3rd term
    % 1st Integral
    wx1 = grad_v2_13_x .* grad_p0_13_x;
    wy1 = grad_v2_13_y .* grad_p0_13_y;
```

```
87      fw1 = fft2( lap_v2_13 .* p0_13 + wx1 + wy1 );
88      fp1 = fft2( p0_23 );
89      int1 = ifft2 ( fw1 .* fp1 );
90      % 2nd Integral
91      wx2 = grad_v2_23_x .* grad_p0_23_x;
92      wy2 = grad_v2_23_y .* grad_p0_23_y;
93      fw2 = fft2( lap_v2_23 .* p0_23 + wx2 + wy2 );
94      fp2 = fft2(p0_13);
95      int2 = ifft2 ( fw2 .* fp2 );
96      % 3rd Integral
97      fwx3 = fft2 ( p0_13 .* grad_v2_13_x);
98      fwy3 = fft2 ( p0_13 .* grad_v2_13_y);
99      fp3 = fp1;
100     intx3 = ifft2( fwx3 .* fp3 );
101     inty3 = ifft2( fwy3 .* fp3 );
102     % 4th Integral
103     fwx4 = fft2 ( p0_23 .* grad_v2_23_x );
104     fwy4 = fft2 ( p0_23 .* grad_v2_23_y );
105     fp4 = fp2;
106     intx4 = ifft2( fwx4 .* fp4 );
107     inty4 = ifft2( fwy4 .* fp4 );
108     % total contributions:
109     integral1 = int1 .* p0_12 * dA;
110     integral2 = int2 .* p0_12 * dA;
111     integral3 = (intx3 .* grad_p0_12_x + inty3 .* grad_p0_12_y
            ) * dA;
112     integral4 = (intx4 .* grad_p0_12_x + inty4 .* grad_p0_12_y
            ) * dA;
113     third = (integral1 + integral2 + integral3 + integral4)./(
            constantP^3);
114     % final step
```

```
115     change = 2 * G * (first + second + third); % dP_12
116     p0_12 = p0_12 + change * step;
117     p0_12 = p0_12 * (N * (N-1) / A) / (sum(sum(p0_12)) * dA);
118     % Data for ploting of p0_12 :
119     if rem(s,ploting_step)== 0;
120     var_plot(:,:,iii) = p0_12;
121     iii = iii+1;
122     end
123     val = sum(sum(abs(change(Filter)/total_step)));
124     abs_delta(end+1) = val;
125     if val > max_delta
126     elseif s > 10000 && (val < max_delta/2) && mean(abs_delta
          ((end-9):(end-5)))-mean(abs_delta(((end-4):end)))< 1e-4
127             disp(['Cut Here: Step = ', num2str(s)])
128             cut = s;
129             break
130     end
131 end
132 % Plot :
133 fig_num = 1;
134 hh = zeros(n,n,total_step/ploting_step);
135 for fig_num = 1: total_step/ploting_step
136     figure(fig_num);
137     hh(fig_num) = surf(y2,x2,var_plot(:,:,fig_num),'edgealpha'
          ,0);
138     colorbar
139     az = 90;
140     el = 90;
141     view([az,el])
142     axis tight
143     title(['Total steps = ',num2str(fig_num * ploting_step),'
```

```
        ','n =',num2str(n),'    ','K_bT =',num2str(KbT),'    ',
        'N =',num2str(N)]);
144     saveas(hh(fig_num),sprintf('figure_Zdirect_%d.jpg',fig_num
        ));
145     az = 90;
146     el = 0;
147     view([az,el])
148     axis tight
149     title(['Total steps = ',num2str(fig_num * ploting_step),'
        ','n =',num2str(n),'    ','K_bT =',num2str(KbT),'    ',
        'N =',num2str(N)]);
150     saveas(hh(fig_num),sprintf('figure_Xdirect_%d.jpg',fig_num
        ));
151     if rem(fig_num,3) == 0
152         close all
153     end
154 end
155 close all
156 save p12_0.1163_450k.m p0_12 v2_12 dA grad_p0_12_x
    grad_p0_12_y grad_v2_12_x grad_v2_12_y lap_v2_12 y2 x2
157 % Plot absolute value Part
158 fig_num = fig_num + 1;
159 figure(fig_num)
160 ps = size(abs_delta);
161 plot_abs = linspace(1,ps(2),ps(2))';
162 h2 = plot(plot_abs,abs_delta);
163 title(['maximum absolute','    ', 'Total steps = ',num2str(
    fig_num * ploting_step),'    ','K_bT =',num2str(KbT),'    ','
    N =',num2str(N)]);
164 saveas(h2,'maximum_absolute.jpg')
```

D.2. One-body Distribution

```
% one-body distribution function :
% Constants
G = 1; % Gama
n = 2000;  % number of grid points
L = 13.52 * 2.866;    % length of simulation cell edge
N = 200;  % number of particles
constantP = N/(L^2);
delta = L/n; % the spacing of the grid
KbT = 0.1163;
beta = 1/KbT;
step = 1e-5;   % length of time step
total_step = 4000000; % total number of steps
ploting_step = 10000;
load GG_0.1163_450k.mat p0_12 v2_12 dA grad_p0_12_x
   grad_p0_12_y grad_v2_12_x grad_v2_12_y lap_v2_12 y2 x2
% adding perturbation to simulation box
p1 = ones(n);
p1 = p1 * N / (sum(sum(p1)) * dA);
noise = 10;
for a = 1:3
    row = randi( n - noise ) + ( 1:noise );
    col = randi( n - noise ) + ( 1:noise );
    p1( row, col ) = p1( row, col ) + 0.01 * p1(1,1) * randn(
       noise );
end
p2 = circshift(p1,[n/2,n/2]);
% Plot the initial case
fig_num = 1;
figure(fig_num);
nn = surf(x2,y2,p1,'edgealpha',0);
```

```
29 title(['Total steps = 1 ','    ','n =',num2str(n),'    ','K_bT =
       ',num2str(KbT),'    ','N =',num2str(N)]);
30 az = 90;
31 el = -90;
32 view([az,el])
33 colorbar
34 axis tight
35 saveas(nn(fig_num),sprintf('figure_initial_noise_%d.jpg',
       fig_num));
36 % one body formulation
37 var_plot = zeros(n,n,total_step/ploting_step);
38 D = zeros(total_step,1);
39 ii =1;
40 % values relates to V_2 that do not change as we iterate to a
       solution:
41 % Integral part 1
42 wx1 = grad_v2_12_x .* grad_p0_12_x;
43 wy1 = grad_v2_12_y .* grad_p0_12_y;
44 fw1 = fft2( lap_v2_12 .* p0_12 + wx1 + wy1 );
45 % Integral part 2
46 wx2 =  (grad_v2_12_x .* p0_12);
47 fwx2 = fft2( wx2 );
48 wy2 =  (grad_v2_12_y .* p0_12);
49 fwy2 =  fft2( wy2  );
50 start =1;
51 for s = start:total_step
52     disp(s)
53     grad_p1_x = nablax(p1,delta);
54     grad_p1_y = nablay(p1,delta);
55     lap_p1 = laplacian3(p1,delta);
56     % 1st term
```

```
57      first = KbT .* lap_p1;
58      % 2nd term
59      fp = fft2( p2 );
60      int1 = ifft2 ( fw1 .* fp );
61      intx2 = ifft2 ( fwx2 .* fp );
62      inty2 = ifft2 ( fwy2 .* fp );
63      % total contribution :
64      integral1 = int1 .* p1 * dA;
65      integral2 = (intx2 .* grad_p1_x + inty2 .* grad_p1_y) * dA
            ;
66      second = (integral1 + integral2)./(constantP ^2);
67      % final step
68      change = G * (first + second); % dP_1
69      p1 = p1 + change * step;
70      p1 = p1 * N / (sum(sum(p1)) * dA);
71      p2 = circshift(p1,[n/2,n/2]);
72      D(s) = max(max(p1)) - min(min(p1));
73      % plot data
74      if rem(s,ploting_step)== 0;
75          var_plot(:,:,ii) = p1;
76          ii = ii+1;
77      end
78  end
79  % PLOT
80  hh = zeros(n,n,total_step/ploting_step);
81  for fig_num = 1: total_step/ploting_step
82  figure(fig_num);
83  hh(fig_num) = surf(x2,y2,var_plot(:,:,fig_num),'edgealpha',0);
84  title(['Total steps = ',num2str(fig_num * ploting_step),'    ',
        'n =',num2str(n),'    ','K_bT =',num2str(KbT),'    ','N =',
        num2str(N)]);
```

```
85 az = 90;
86 el = -90;
87 view([az,el])
88 colorbar
89 axis tight
90 saveas(hh(fig_num),sprintf('figure_noise_%d.jpg',fig_num));
91 if rem(fig_num,3) == 0
92     close all
93 end
94 end
95 % save onebody p1 var_plot
96 save P_1_0.1163.m p1 p2
```